UNIVERSITY OF CALIFORNIA SAN DIEGO

The Role of Circadian Disruption in Mediating Non-Alcoholic Steatohepatitis in the Streptozotocin/High-Fat Diet Murine Model

A dissertation submitted in partial satisfaction of the requirements for the degree Doctor of Philosophy

in

Biomedical Sciences

by

Kelly Anne Fogelson

Committee in charge:

Professor Rob Knight, Co-Chair
Professor Amir Zarrinpar, Co-Chair
Professor David Gonzalez
Professor Dorothy Sears

2022

The dissertation of Kelly Anne Fogelson is approved, and it is acceptable in quality and form for publication on microfilm and electronically.

University of California San Diego

2022

Dedication

To my parents,

Whose sacrifices have paved the way for me to pursue every opportunity,

be wildly curious,

and dream bigger.

Whose love continues to push me to believe in myself.

It is a tremendous honor and privilege to be the first in our family line to achieve the title of

“**doctor**”.

The completion of this body of work,

and the countless years leading up to it,

are dedicated to you.

Epigraph

“The beginning of knowledge is the discovery of something we do not understand.”

– Frank Herbert

Table of Contents

Dissertation Approval Page …… iii

Dedication …… iv

Epigraph …… v

Table of Contents …… vi

List of Abbreviations ……..…… viii

List of Figures ……..……..…. ix

List of Tables ……..…….. x

Acknowledgements ……..……..…….. xi

Vita ……..……..……..... xii

Abstract of the Dissertation ……..……..... xiii

Introduction …..……..……..…….. 1

Chapter 1. Research Premise: Non-Alcoholic Steatohepatitis,

the Gut Microbiome, and Circadian Rhythms ……..……. 4

Chapter 1.1. The Importance of the Clinical Problem and Barriers to Progress …….. 5

Chapter 1.2. Filling Knowledge Gaps and Scientific Premise ……. 6

Chapter 1.2.a. The Streptozotocin + High Fat Diet Model of NASH ……. 6

Chapter 1.2.b. NASH and Circadian Rhythms ……. 7

Chapter 1.2.c. The Metabolic Effects of Circadian Dyssynchrony …… 7

Chapter 1.2.d. The Gut Microbiome and Circadian Rhythms …… 8

Chapter 1.2.e. The Gut Microbiome and Bile Acid Signaling …… 9

Chapter 1.2.f. Bile Acid Signaling and NASH …….. 11

Chapter 1.2.g. The Impact of Time-Restricted Feeding on Host Physiology.. 12

Chapter 2. The Effect of NASH on Feeding, Gut Microbiome,

and Gut Microbial Metabolome Rhythms…… 17

Chapter 2.1. Research Design …… 18
Chapter 2.2. Time-Restricted Feeding Does Not Protect Against STAM/HFD-Induced NASH..……. 18
Chapter 2.3. STAM/HFD-Induced NASH Does Not Disrupt Feeding Rhythms …….. 20
Chapter 2.4. Mice with STAM/HFD-Induced NASH on Adlib Feeding Have Disrupted Diurnal Fluctuations in Stool Microbiome Composition …… 20
Chapter 2.5. Mice with STAM/HFD-Induced NASH on Adlib Feeding Have Disrupted Diurnal Fluctuations in Ileum Microbiome Composition …… 22
Chapter 2.6. Mice with STAM/HFD-Induced NASH Have Disrupted Diurnal Fluctuations in Stool Metabolome …… 23
Chapter 2.7. Discussion …… 25
Chapter 2.8. Research Methods …… 28
Chapter 2.8.a. Experimental Methods …… 28
Chapter 2.8.b. Data and Statistical Analysis ……..…… 32
Chapter 3. The Effect of NASH on Diurnal Transcriptional Patterns in the Ileum and Liver … 52
Chapter 3.1. Diurnal Transcriptional Patterns are Maintained in the Ileum During STAM/HFD-Induced NASH …… 53
Chapter 3.2. Diurnal Transcriptional Patterns are Maintained in the Liver During STAM/HFD-Induced NASH …… 55
Chapter 3.3. Discussion …… 57
Chapter 3.4. Research Methods …….. 57
Chapter 3.4.a. Experimental Methods …… 57
Chapter 3.4.b. Data and Statistical Analysis ……..…… 58
Summary ……..…… 68
References ……..…… 69

List of Abbreviations

Abbreviation	Definition
Adlib	*Ad libitum*
BSH	Bile salt hydrolase
FA	High-fat diet + adlib access to food
FT	High-fat diet + TRF access food
HCC	Hepatocellular carcinoma
HFD	High fat diet
H&E	Hematoxylin and eosin
MetS	Metabolic syndrome
NA	Normal chow diet + *ad libitum* access to food
NAFL	Non-progressive simple steatosis
NAFLD	Non-alcoholic fatty liver disease
NAS	NAFLD activity score
NASH	Non-alcoholic steatohepatitis
NCD	Normal chow diet
STAM	Streptozotocin
STAM/HFD	Streptozotocin + high-fat diet
TRF	Time-restricted feeding

List of Figures

Figure 1. Bacterial Bile Acid Biotransformations …… 14

Figure 2. Experimental Design ……. 36

Figure 3. Time-Restricted Feeding Does Not Prevent STAM/HFD-Induced NASH …….. 37

Figure 4. STAM/HFD-Induced NASH Does Not Disrupt Feeding Rhythms ……... 38

Figure 5. FA Results in Disrupted Diurnal Fluctuations in Stool Microbiome Composition 40

Figure 6. FA Results in Disrupted Diurnal Fluctuations in Ileum Microbiome Composition 42

Figure 7. STAM-Induced NASH Results in Disrupted Fluctuations in Stool Metabolome … 44

Figure 8. Diurnal Transcriptional Patterns in the Ileum are Maintained During STAM/HFD-induced NASH …….. 59

Figure 9. Diurnal Transcriptional Patterns in the Liver are Maintained During STAM/HFD-induced NASH …….. 63

Supplemental Figure 1. Individual Animal Traces for Behavioral Rhythms …….. 39

Supplemental Figure 2. Additional 16S Composition Measurements – Stool …….. 41

Supplemental Figure 3. Additional 16S Composition Measurements – Ileum ……. 43

Supplemental Figure 4. Additional Stool Metabolomics Measurements …….. 47

Supplemental Figure 5. Liver Transcriptomics Heat Map …… 66

List of Tables

Table 1. Physiological Processes Affected by Bile Acid Receptor Signaling ……. 15

Acknowledgements

I would like to acknowledge Professor Rob Knight and Professor Amir Zarrinpar for their support as co-chairs of my committee. Their support and unwavering encouragement has been fundamental to my success in ultimately completing my doctoral thesis. I would also like to acknowledge Professor David Gonzalez and Professor Dorothy Sears for serving as members on my committee. Their feedback has been invaluable to improving the quality and rigor of my doctoral thesis.

Chapter 1 includes portions of text that are in review for publication: “Fogelson, Kelly; Dorrestein, Pieter; Zarrinpar, Amir; Knight, Rob. The Gut Microbial Bile Acid Modulation and its Relevance to Digestive Health and Diseases. (In review at Gastroenterology)”. The dissertation author is the primary investigator and author of this paper.

Chapter 2 is currently being prepared for submission for publication of the material: “Fogelson, Kelly; Aron, Allegra; Muti, Valentina; Salido Benítez, Rodolfo Antonio; Richter, Roland; Hu, Jingjing; Hosseini, Mojgan; Dorrestein, Pieter; Knight, Rob; Zarrinpar, Amir. Title and Journal Undetermined. (Paper currently in preparation).” The dissertation author is the primary investigator and author of this paper.

Chapter 3 is currently being prepared for submission for publication of the material: “Fogelson, Kelly; Aron, Allegra; Muti, Valentina; Salido Benítez, Rodolfo Antonio; Richter, Roland; Hu, Jingjing; Hosseini, Mojgan; Dorrestein, Pieter; Knight, Rob; Zarrinpar, Amir. Title and Journal Undetermined. (Paper currently in preparation).” The dissertation author is the primary investigator and author of this paper.

Vita

2013-2017	Bachelor of Science, The University of Minnesota, Twin Cities
2018-2019	Post-Baccalaureate Research Education Scholar, The Johns Hopkins University School of Medicine
2019-2022	Doctor of Philosophy, University of California San Diego

Abstract of the Dissertation

The Role of Circadian Disruption in Mediating Non-Alcoholic Steatohepatitis in the Streptozotocin/High-Fat Diet Murine Model

by

Kelly Anne Fogelson

Doctor of Philosophy in Biomedical Sciences

University of California San Diego, 2022

Professor Rob Knight, Co-Chair
Professor Amir Zarrinpar, Co-Chair

Non-alcoholic fatty liver disease (NAFLD) has rapidly emerged as the most prevalent liver disease in westernized countries, affecting approximately 1 in 3 adults in the US and roughly 25% of adults globally [1,2]. NAFLD can progress to nonalcoholic steatohepatitis (NASH), a progressive form of the disease characterized by inflammation, hepatocyte injury, and increased risk for hepatology-related morbidity and mortality [3]. It is unclear why only a subset of patients with NAFLD progress to NASH. One of the leading explanations is the "multiple parallel hits hypothesis", which considers multiple insults such as hepatic steatosis,

inflammation, and insulin resistance that act in unison to trigger the progression of NAFLD to NASH [4]. However, a very significant element of this hypothesis that is missing is circadian rhythms, which play a role in modulating every insult or “hit”. Our objective is to elucidate the role of circadian rhythms in the liver and intestines, which can be entrained by the gut microbiome, in the pathophysiology and progression of NAFLD to NASH. Previous research indicates that certain feeding patterns, such as time-restricted feeding (TRF), prevent a variety of NASH risk factors, including hepatic steatosis and circadian rhythm disruption in the liver and intestines [5,6]. We hypothesize that NASH onset results from altered gut microbiome dynamics and disrupted hepatic circadian rhythms, which can be manipulated with feeding pattern to ameliorate disease. To test this hypothesis, we used the streptozotocin + high-fat diet (STAM/HFD) murine model of NASH, which recapitulates key aspects of human NASH pathogenesis, including hepatic steatosis, inflammation, and fibrosis on a hyperglycemic background [7]. STAM/HFD mice underwent 8-hour TRF or had access to food *ad libitum* (adlib). Importantly, STAM/HFD mice are hypoinsulinemic and do not become insulin resistant [7]. This allowed us to specifically investigate whether TRF can prevent NASH via the modulation of circadian rhythms, without the confounding factor of TRF affecting insulin signaling. Our results demonstrate that TRF is not capable of preventing NASH in the STAM/HFD model. Surprisingly, STAM/HFD mice with adlib access to food have a maintenance of rhythmic feeding patterns, as well as a maintenance of ileal and hepatic gene expression patterns. TRF was capable of preventing disruptions to diurnal fluctuations in gut microbiome composition. However, this was not capable of preventing the onset of NASH in the STAM/HFD model. Results from this study suggest that STAM/HFD-induced NASH does not result from circadian rhythm disruption, and that insulin may be a crucial element to mediating the protective effects of TRF.

Introduction

Non-alcoholic fatty liver disease (NAFLD) is the most prevalent liver disease in westernized countries and affects approximately 1 in 3 adults in the US [1,2]. NAFLD presents as a spectrum of liver diseases and is characterized by hepatic fat accumulation in the absence of other causes of steatosis (e.g., alcohol, hepatitis B/C virus) [1]. NAFLD is thought to be the hepatic manifestation of metabolic syndrome (MetS), and thus, is closely associated with obesity, type 2 diabetes, and cardiovascular disease [8]. Approximately 1 in 4 people with NAFLD, or about 6% of the US population, develops non-alcoholic steatohepatitis (NASH), a progressive form of NAFLD that is characterized by fat plus inflammation and scarring [3]. NASH is an important turning point in the NAFLD disease spectrum. NASH greatly increases the risk of developing advanced stages of disease, such as cirrhosis and hepatocellular carcinoma (HCC), which cause irreversible liver damage and increase hepatology-related mortality risk [3]. Despite its prevalence, there are no therapies designed specifically for the treatment of NASH. Typically, treatments that address comorbid conditions, such as weight loss and lifestyle changes for obesity and type 2 diabetes (e.g., physical exercise, diet modification) are recommended for individuals suffering from NASH [8]. However, long-term weight loss of sufficient quantity to reverse NASH has proven to be unachievable for the majority of patients in clinical studies [9]. Furthermore, pharmacological interventions capable of reversing NASH through weight loss, or the lowering of blood glucose, lipids, or inflammation have also shown little efficacy [8]. Hence, NASH is a serious chronic condition with treatments that either lack efficacy or are unattainable for most patients.

It is widely unknown why only a subset of patients with NAFLD progress to NASH. One of the leading explanations is the “multiple parallel hits” hypothesis, which considers multiple insults acting in unison to trigger the progression of NAFLD to NASH [4]. Some of the hits included in this hypothesis are dietary, environmental, and genetic factors, insulin resistance,

inflammation, hepatic steatosis, and changes to the gut microbiome [4]. However, a very significant element of this hypothesis that is missing is the effect of circadian rhythms. Circadian rhythms are a core set of cellular processes and physiological behaviors under the regulation of circadian clock proteins. Circadian rhythms play a key role in regulating every insult, or “hit”, included in the multiple parallel hits hypothesis. In humans, disruption of circadian behaviors, as in shift-work, have been linked to dysmetabolic states that increase NASH susceptibility (e.g., obesity, type 2 diabetes, hypertension) [10]. The pathophysiological mechanisms of NASH are multifactorial, but occur in the context of dysregulated metabolic processes such as glucose, lipid, and bile acid dysmetabolism [11]. These metabolic processes are modulated by master metabolic regulators in the liver (e.g., CREB, mTOR, AMPK) that have cyclical activity, and can regulate, and be regulated by, circadian clock proteins (e.g., CLOCK:BMAL1, PER, CRY) [12]. Importantly, previous research demonstrates that the gut microbiome is required for normal circadian cycling of these metabolic regulators and of the hepatic circadian clock [13]. Further, mouse and human studies demonstrate that NASH is associated with compositional changes in the gut microbiome [14,15]. However, 24hr changes in gut microbiome composition during NASH have yet to be characterized, and the precise mechanisms of how dysregulated circadian rhythms in the liver and intestines contribute to the pathophysiology of NASH remain widely unknown.

Consolidating food intake to a defined period of the day with time-restricted feeding (TRF) is a powerful metabolic tool that has been shown to prevent a variety of risk factors for NASH. Recent human studies indicate that TRF improves a cluster of conditions that could reduce NASH susceptibility, including weight, blood pressure, and atherogenic lipid profiles [10]. Further, studies in murine models of diet-induced obesity show that TRF reduces insulin resistance, adiposity, inflammation, liver steatosis, and corrects circadian dyssynchrony across multiple sites in the host [5,6,16]. Although the mechanisms of TRF are not well understood, it is

hypothesized that TRF could exert its therapeutic effects through modulation of the gut microbiome and restoration of circadian rhythms [5,6,16]. Thus, our central hypothesis is that NASH pathogenesis is associated with disrupted host circadian rhythms, including feeding rhythms, gut microbiota dynamics, as well as hepatic and intestinal transcriptional rhythms, which can be manipulated with TRF to ameliorate disease. To address this hypothesis, we investigated the diurnal dynamics of feeding, transcriptional, and gut microbiota rhythms under *ad libitum* (adlib) and 8-hour TRF in mice with streptozotocin + high-fat diet (STAM/HFD)-induced NASH. Our goal was to characterize circadian rhythms across multiple sites in the host before and during NASH onset under adlib and TRF, and determine how circadian dyssynchrony correlates with disease outcomes. Importantly, STAM/HFD mice are hypoinsulinemic and therefore do not become insulin resistant [7]. This enabled us to specifically investigate whether TRF can prevent NASH via the modulation of circadian rhythms, without the confounding effects of TRF affecting insulin signaling.

Our results demonstrate that mice with STAM/HFD-induced NASH have a maintenance of rhythmic feeding patterns, as well as a maintenance of ileal and hepatic gene expression patterns. TRF is capable of preventing disruptions to diurnal fluctuations in gut microbiome composition in mice with STAM/HFD-induced NASH. However, TRF is not capable of preventing NASH in the STAM/HFD model. Results from this study suggest that STAM/HFD-induced NASH does not result from circadian rhythm disruption, and that insulin may be critical to mediating the protective effects of TRF.

Chapter I

Research Premise: Non-Alcoholic Steatohepatitis,
the Gut Microbiome, and Circadian Rhythms

1.1. The Importance of the Clinical Problem and Barriers to Progress

NAFLD presents as a spectrum of liver diseases that can generally be grouped into two categories: non-progressive simple steatosis (NAFL), and NASH, a progressive form of NAFLD which is characterized by inflammation and hepatocyte injury [17]. Although NAFL carries little risk of advancing to progressive stages, NASH greatly increases the risk of irreversible liver damage as well as the risk of hepatology-related mortality from cirrhosis and HCC [18]. Approximately 20 million people in the US, or ~6% of the population, suffer from NASH [3]. NASH is one of the last reversible stages of the NAFLD disease spectrum [8]. Thus, the development of novel therapeutics capable of preventing and/or treating NASH could greatly reduce hepatology related morbidity and mortality. NASH is associated with MetS, a cluster of conditions including obesity, insulin resistance, hypertension, and dyslipidemia [8]. Currently, there are no treatments designed specifically for NASH. Instead, individuals are treated for the symptoms associated with NASH, such as excess weight (e.g., physical exercise, diet modification). However, long-term weight loss of sufficient quantity to reverse NASH has proven difficult for most patients in clinical studies [9]. Thus, novel therapeutics for the treatment of NASH are needed.

It is widely unknown why only a subset of patients with NAFLD progress to NASH. The leading explanation for what triggers this progression is the “multiple parallel hits hypothesis”, which considers multiple insults acting in unison to trigger the advancement of NAFLD to NASH [4]. Some of the insults, or “hits”, included in this hypothesis are dietary, environmental, and genetic factors, insulin resistance, inflammation, hepatic steatosis, and changes to the gut microbiome [4]. However, a very significant element that is missing is the effect of circadian rhythms, which play a crucial role in regulating every insult included in the multiple parallel hits hypothesis.

1.2. Filling Knowledge Gaps and Scientific Premise

1.2.a. The Streptozotocin + High Fat Diet Model of NASH

In our studies, we will use the streptozotocin (STAM) + high-fat diet (HFD) model (STAM/HFD) of NASH. In this model, neonatal C57BL/6 male mice are injected subcutaneously with low-dose STAM [7]. STAM is an alkylating agent that is clinically used to treat pancreatic beta cell carcinoma in humans [19]. In mice, low-dose STAM administered postnatally is toxic to pancreatic beta cells, which rapidly proliferate during the neonatal period [19]. STAM is similar to glucose in structure. Thus, STAM is transported into pancreatic beta cells via the glucose transport protein GLUT2, which is highly expressed in this tissue. Destruction of pancreatic beta cells postnatally results in hypoinsulinemia and hyperglycemia, effectively leaving mice with a type I diabetes phenotype. At 4 weeks old, STAM-primed mice begin HFD (60% Kcal fat). The combination of chemical and dietary insults induces sequential histological changes from simple steatosis, to inflammation, fibrosis, and NASH, which recapitulates key stages of disease progression that are observed in humans. In this model, male mice display NAFLD at 6-8 weeks and NASH at 10-12 weeks. This model shows 100% reproducibility in male mice with a clear disease time course that is short compared to other models of NASH [20,21].

In the STAM/HFD model, persistent hyperglycemia and HFD increases hepatic fat deposition, leading to increased lipogenesis, fatty acid oxidation, and oxidative stress in the mouse liver. Resulting hepatocyte injury leads to macrophage recruitment and the formation of inflammatory foci that phagocytose lipid droplets [7]. This phenomenon decreases as the mice age, which mirrors trends seen in human NASH where macrophage function is altered at later stages of inflammation. Overall, this model recapitulates key aspects of NASH pathogenesis that are observed in humans and presents a reliable model of NASH on a diabetic background for use in this study.

1.2.b. NASH and Circadian Rhythms

Circadian rhythms are a core set of cellular processes and physiological behaviors under the regulation of circadian clock proteins (e.g., CLOCK:BMAL1, PER, CRY). They help coordinate internal physiological processes with external environmental events [12]. Normal functioning of the circadian clock is a required component of health [22]. Circadian clock proteins maintain 24-hr rhythms under constant conditions, yet have the ability to be entrained by environmental cues (e.g., feeding, temperature) [23]. In mammals, the suprachiasmatic nucleus is the central circadian clock and is entrained by light [12]. However, circadian rhythms are not restricted to the central circadian clock. In mammals, circadian clock proteins are expressed in nearly every cell of the body [12]. Daily oscillations in circadian clock proteins are active in peripheral tissues such as the liver. Feeding/fasting cycles are critical to the entertainment of hepatic circadian rhythms.

The pathophysiological mechanisms of NASH are multifactorial, but occur in the context of dysregulated metabolic processes such as glucose, lipid, and bile acid dysmetabolism [11]. These metabolic processes are modulated by master metabolic regulators in the liver (e.g., CREB, mTOR, AMPK) that have cyclical activity, and can regulate, and be regulated by, circadian clock proteins [12]. Thus, the circadian clock is critically linked to host metabolic processes. In humans, disruption of circadian behaviors, as in shift-work, has been linked to dysmetabolic states that increase NASH susceptibility (e.g., obesity, type 2 diabetes, hypertension) [10]. Altogether, dysregulated circadian rhythms have emerged as a key contributor to NASH pathogenesis [12].

1.2.c. The Metabolic Effects of Circadian Dyssynchrony

Circadian dyssynchrony can be characterized as dampened and/or phase-shifted expression of clock oscillator genes, along with their lack of synchronization with cellular

metabolic regulators. Circadian dyssynchrony can also be quantified as dampened and/or phase-shifted shifted oscillation of 24hr host rhythms, such as feeding patterns, energy expenditure, and diurnal changes in gut microbiome composition. Circadian dyssynchrony is a hallmark of MetS, cardiovascular disease, and inflammation, and is observed in animal models where dysmetabolic states (e.g obesity, NAFLD, hyperlipidemia) are induced by diet (e.g., high-fat and high-sucrose diets) [6,16]. Thus, circadian dyssynchrony plays an important role in dysmetabolic states that are closely associated with NASH.

1.2.d. The Gut Microbiome and Circadian Rhythms

The gut microbiota refers to a collection of organisms living in the gastrointestinal tract, including bacteria, fungi, viruses, and other organisms, whereas the gut microbiome refers to both the gut microbiota and the collective interacting genomes of various community members. Recent estimates find that humans have approximately 1.3x more bacterial cells than human cells, and a staggering 100x more microbial genes in the gut microbiome than the entire human genome [24,25]. Weighing in at approximately 3-5 pounds of bacteria, the importance of the gut microbial ecosystem on influencing human health and disease cannot be understated [26]. Importantly, the composition of the gut microbiome is not static, but rather, highly dynamic. The gut microbiome exhibits diurnal patterns that are closely tied to and appear to be required for maintenance of normal host circadian rhythms and metabolic homeostasis [5,27]. Indeed, circadian disruption induced by jet-lag [28], genetic mutation of host circadian genes [28–30], or by feeding high-fat diet (HFD) [5,27] are associated with disruptions in microbe-host circadian dynamics that can result in increased adiposity, insulin resistance, and inflammation [31]. Peripheral circadian rhythms are perturbed in germ-free mice [27,32]. However, with a transplant of a conventional gut microbiome, they gain circadian oscillation of at least their hepatic clock components. Hence, it appears that the gut microbiome is required for maintenance of normal

hepatic circadian rhythms and host metabolic homeostasis. In fact, luminal cues are better at entraining hepatic circadian rhythms than the more canonical clock mechanisms [33].

1.2.e. The Gut Microbiome and Bile Acid Signaling

Mouse and human studies demonstrate that NASH is associated with compositional changes in the gut microbiome [14,15]. However, 24hr changes in gut microbiome composition during NASH have yet to be characterized. Additionally, the mechanisms by which the gut microbiome affects NASH formation, and the signals used to mediate their effects, are largely unknown. Bile acids (BAs) may serve as the signal linking luminal bacteria and host metabolic processes during NASH. The BA signaling cycle is initiated in the liver (**Fig 1**). Conjugated BAs, synthesized from cholesterol and released by the liver, are vital for micelle formation, lipid solubilization and absorption, and cholesterol homeostasis [34,35]. BAs are produced in the liver by *de novo* conversion of cholesterol to cholic acid (CA) and chenodeoxycholic acid (CDCA) by cholesterol 7-α-hydroxylase (CYP7A1). In rodents, CDCA is further metabolized to muricholic acids (MCAs) [36]. Before excretion into bile, BAs are primarily conjugated with taurine or glycine in humans, although many new conjugated BAs and microbes that conjugate or deconjugate them have recently been discovered through the combination of untargeted mass spectrometry based metabolomics, genome sequencing, and lab experiments on individual strains [37–42].

Because of their detergent properties, BAs can damage bacterial cell walls and modify the microbiome by restricting growth or survival of specific bacterial taxa. Many gut bacterial species in the proximal small intestine are BA resistant or have developed strategies to modify BAs to protect themselves [35,43]. Bile salt hydrolase (BSH), an enzyme specific to bacteria, deconjugates BAs and thereby weakens their detergent properties [44]. Although the host has a dedicated BA transporter for conjugated BAs, the apical sodium–BA transporter (ASBT),

deconjugated BAs do not have transporters and are reabsorbed with more difficulty through passive diffusion [36]. Thus, bacterial deconjugation of primary conjugated BAs promotes the excretion or retention of deconjugated BAs in the lumen to the distal colon where other bacteria can use them as substrates. Deconjugated BAs become available for further biotransformations by other bacteria, yielding secondary BAs including deoxycholic acid (DCA), ursodeoxycholic acid (UDCA), and lithocholic acid (LCA) [43,45]. Although much of this hydrophobic pool of secondary BAs is excreted, enough is absorbed through passive diffusion to change the serum BA pool and act as signaling molecules [46]. Deconjugated and secondary BAs are absent in germ-free mice [47–50], and heavily decreased in antibiotic-treated, microbiome-depleted mice [51], proving that the microbiome produces them.

Deconjugated and secondary BAs serve as important signaling molecules that affect a number of physiological processes, including cholesterol, lipid, and glucose homeostasis [36]. BAs act as agonists and antagonists to BA receptors (**Fig 1**). BA signaling pathways, including the nuclear hormone receptor farnesoid X receptor (FXR) [52] and the G protein-coupled BA receptor 1 (TGR5) [53], are potent metabolic regulatory pathways that are highly conserved between mouse models and humans (**Table 1**). BAs also activate other nuclear hormone receptors, including pregnane-x-receptor (PXR), constitutive androstane receptor (CAR), vitamin D receptor (VDR), liver-X-receptor α and β (LXRα/β, NR1H3), RAR-related orphan receptor γt (RORγt), and G-protein-coupled receptors including the sphingosine 1-phosphate receptor 2 (S1PR2) [54], broadening their functional reach. FXR is most highly expressed in the liver, ileum, and kidneys, and to a lesser extent in peripheral tissues such as the heart, ovary, thymus, eye, spleen, immune cells, neural tissue, and testes [36]. Although FXR has broad impacts on host metabolic processes, its most well-studied roles relate to its regulation of primary BA synthesis from cholesterol by the liver [52]. TGR5 is found in intestinal L-cells, immune cells such as Kupffer cells, and muscle and brown adipose tissue (BAT) [36]. Additionally, TGR5 is

highly expressed in the gallbladder, lungs, spleen, liver, bone marrow, and placenta [36]. Broadly, BA-activated TGR5 in peripheral tissues is most well-studied for its role in modulating host energy homeostasis. Importantly, BAs have highly disparate diurnal fluctuations, particularly BAs in the ileum [55], and are potential entrainment signals of intestinal and hepatic circadian rhythms [13,56,57]. Thus, they can have an outsized role in a wide array of homeostatic and physiological processes, as well as conditions where circadian rhythms have a pathophysiological role. Hence, deconjugated and secondary bile acids are prime candidates for being entraining agents of peripheral circadian rhythms and may play an important role in mediating the metabolic effects of the gut microbiome during NASH.

1.2.f. Bile Acid Signaling and NASH

Dysregulation of bile acid homeostasis has been observed in patients along the disease spectrum of NAFLD to HCC [58,59]. The expression of FXR has been found to be down-regulated during NASH development [60], and knocking out the FXR receptor in mice results in cholestasis (i.e., reduced bile flow from the liver), disrupted cholesterol homeostasis, increased NASH development, and spontaneous HCC formation [61]. Thus, FXR has become an important therapeutic target in battling NASH and its advancement to HCC. FXR activation in the liver inhibits the expression of cholesterol 7-alpha hydroxylase (Cyp7a1), the rate limiting enzyme in the *de novo* synthesis of BAs from cholesterol [36]. Further, FXR activation in the murine ileal enterocytes induces expression of fibroblast growth factor 15 (Fgf15; FGF19 in humans) which also suppresses Cyp7a1 [62,63]. In addition to bile acid homeostasis, other key functions of FXR include regulation of inflammation, and the modulation of glucose, cholesterol, and lipid homeostasis [36]. Overall, these findings suggest that NASH may promote a luminal environment with a greater proportion of BAs that function as FXR antagonists. Therapeutic interventions that could modulate the ratio of antagonists:agonists, such as BSH, could play a therapeutic role in treating NASH.

1.2.g. The Impact of Time-Restricted Feeding on Host Physiology

For the purpose of this study, time-restricted feeding (TRF) can be defined as restricting food intake to a defined period of the active phase. Time-restricted feeding (TRF) is a powerful metabolic tool that is capable of modulating host circadian rhythms [5]. In mice fed a high-fat diet (61% Kcal fat), TRF (Zeitgeber Time [ZT] 13-21) prevents obesity, improves insulin sensitivity, decreases serum cholesterol, triglycerides, and inflammation, increases exercise tolerance, and restores diurnal oscillations in gut microbiome composition [5,6]. Recent human studies indicate that TRF (10-hour restricted eating) is capable of reducing weight, blood pressure, and atherogenic lipid profiles in individuals with MetS [10]. Importantly, in multiple murine models of diet-induced dysmetabolism (e.g., high-fat diet, high-fructose + high-sucrose diet), TRF (ZT13-22) protects against hepatic steatosis and liver damage, which are key precursors to NASH development [16]. Additionally, TRF is a powerful modulator of BA metabolism. TRF is associated with increased expression of hepatic Cyp7a1, an increase in hepatic BAs, and reductions in serum cholesterol [6]. As TRF protects against a variety of metabolic insults and disease states that are closely associated with NASH, we suspect that therapies targeted at correcting circadian dyssynchrony hold great potential for treating diseases along the spectrum of NAFLD to NASH.

It is important to note that previous studies that find TRF to prevent NASH risk factors, including steatosis and disrupted circadian rhythms, were conducted in mouse models of diet-induced obesity where mice are insulin resistant. Insulin is an important aspect of NASH pathogenesis, and one of the key insults included in the multiple parallel hits hypothesis [4]. For the purposes of our study, we specifically want to investigate whether TRF can prevent the development of NASH via the modulation of circadian rhythms. Thus, in the STAM/HFD model where mice are hypoinsulinemic, and therefore do not become insulin resistant, we can study

the true effect that TRF has on circadian rhythms during NASH without the confounding factor of TRF also affecting insulin signaling.

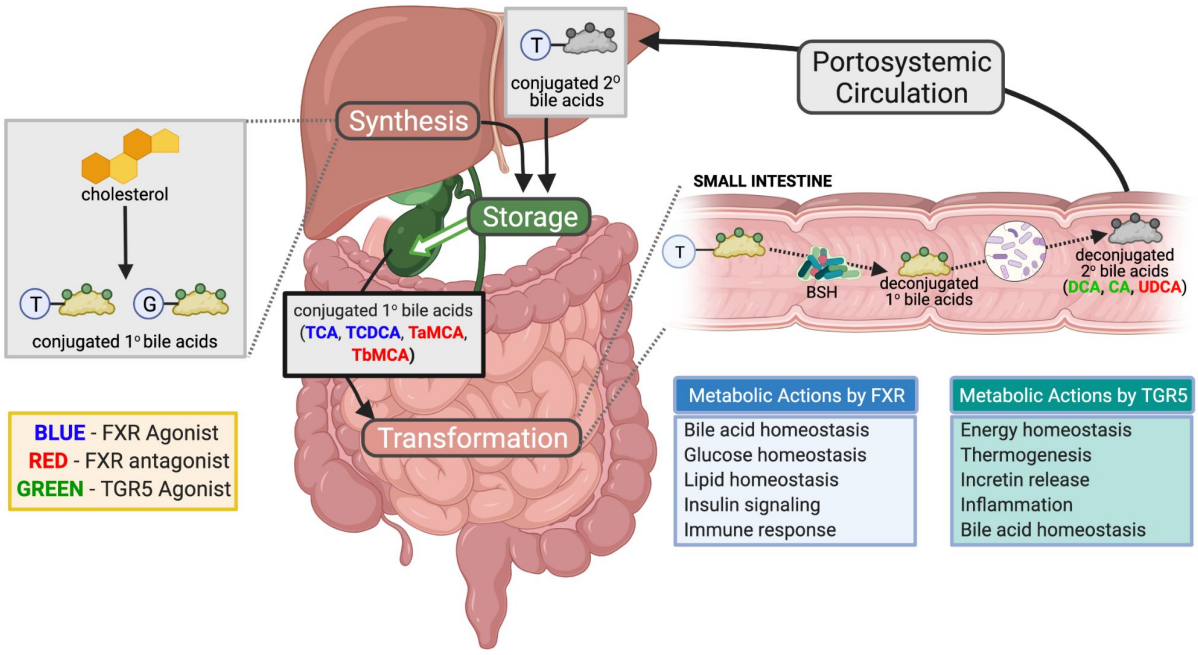

Figure 1. Bacterial Bile Acid Biotransformations
Cholesterol is converted to primary bile acids in the liver. Primary bile acids are conjugated with primarily taurine in mice or glycine in humans before being transported to the gallbladder for storage in the form of bile. Upon ingestion of dietary fats, primary conjugated bile acids (within bile) are released into the gut lumen to aid lipid absorption. Bacteria with bile salt hydrolase deconjugate bile acids, thereby weakening their soap-like qualities. This allows other microbiome members to further modify them into secondary bile acids. Some secondary bile acids can be transported back to the liver, where they are then conjugated. Thus, the interaction between the gut microbiome and bile acids leads to modulation of FXR and TGR5 agonists and antagonists, and thus, allows the gut microbiome to affect host metabolism. (T= taurine, G= glycine, In humans: TCA= taurocholic acid, CA= cholic acid, TCDCA= taurochenodeoxycholic acid, DCA= deoxycholic acid, UDCA= ursodeoxycholic acid, In mice: TaMCA= tauro-α-muricholic acid , TbMCA= tauro-β-muricholic acid, FXR= farnesoid X receptor, TGR5= G-protein-coupled bile acid receptor). Graphic Illustration Source: BioRender.

Table 1. Physiological Processes Affected by Bile Acid Receptor Signaling

Physiological Process	Receptors	Action
Glucose homeostasis	FXR	● Intestinal FXR activation induces FGF-15/FGF-19 secretion, which increases glycogenesis, and inhibits GLP-1 production ● Intestinal FXR modulates glucose absorption and postprandial glucose utilization
	TGR5	● TGR5 increases GLP-1 release in intestinal L-cells, resulting in increased energy expenditure in brown adipose tissue and muscle
Bile acid homeostasis	FXR	● Activation of hepatic FXR inhibits de novo bile acid synthesis in the liver. ● FXR activation in the gastrointestinal tract inhibits de novo bile acid synthesis in the liver via FGF-15/FGF-19 signaling. Inhibition of de novo bile acid synthesis increases hepatic cholesterol
Lipid homeostasis	FXR	● FXR activation increases WAT browning
	TGR5	● TGR5 increases energy expenditure in BAT through the TGR5–cAMP–D2 signaling pathway
Insulin Signaling	FXR	● Pancreatic FXR positively regulates insulin synthesis and glucose-induced insulin secretion
	TGR5	● Pancreatic TGR5 positively regulates insulin synthesis and glucose-induced insulin secretion ● Intestinal TGR5 activation improves glycemic control by GLP-1 release in intestinal L-cells, which increases postprandial insulin secretion from pancreatic beta cells
Inflammation	FXR	● FXR activation inhibits inflammatory cytokine production in the gastrointestinal tract and improves intestinal barrier integrity
	TGR5	● TGR5 activation protects against LPS-induced inflammation

Chapter 1 includes portions of text that are in review for publication: “Fogelson, Kelly; Dorrestein, Pieter; Zarrinpar, Amir; Knight, Rob. The Gut Microbial Bile Acid Modulation and its Relevance to Digestive Health and Diseases. (In review at Gastroenterology)”. The dissertation author is the primary investigator and author of this paper.

Chapter II

The Effect of NASH on Feeding, Gut Microbiome, and Gut Microbial Metabolome Rhythms

2.1. Research Design

The overall goal of this study is to elucidate the role of hepatic circadian rhythms and gut microbiome dynamics in the pathophysiology and progression of NAFLD-associated NASH. Our central hypothesis is that NASH pathogenesis is associated with disrupted host circadian rhythms, including feeding rhythms, gut microbiome and metabolome rhythms, as well as hepatic and intestinal transcriptional rhythms, which can be manipulated with TRF to ameliorate disease. To address this hypothesis, we investigated the diurnal dynamics of behavioral, transcriptional, and microbiota luminal rhythms under adlib and TRF in mice with STAM/HFD-induced NASH (**Fig 2**). Our goal was to characterize circadian rhythms across multiple sites in the host before and during NASH onset under adlib and TRF, and determine how circadian rhythm disruption correlates with disease outcomes.

2.2. Time-Restricted Feeding Does Not Protect Against STAM/HFD-Induced NASH

Previous studies demonstrate TRF protects against a wide variety of metabolic insults and disease states that are closely associated with NASH, including (in mouse studies) 1) hepatic steatosis and liver damage, 2) obesity, 3) insulin resistance, 4) elevated serum cholesterol, triglycerides, and inflammation, 6) disruptions to diurnal gut microbiome rhythms, and (in human studies in individuals with MetS) 7) excess weight, 8) elevated blood pressure, and 9) atherogenic lipid profiles (**Chapter 1.2.g**) [5,6,10,16]. However, whether TRF can prevent NASH remains unknown.

Previous research demonstrates that the STAM/HFD model develops NASH by roughly 12 weeks of age, whereas STAM mice on normal chow diet (STAM/NCD) do not [7]. Thus, to investigate the effects of TRF on STAM/HFD-induced NASH, the phenotype of STAM/HFD mice with TRF access to food from ZT1-ZT13 (FT) was compared to mice with STAM/HFD mice with adlib access to food (FA) and STAM/NCD mice with adlib access to food (NA) (Experimental design **Chapter 1, Fig 2**). Cage-averaged food consumption and individual mouse weights were

recorded over the duration of the experiment (**Fig 3a, Fig 3b)**. Mice in the FT condition have access to food from ZT1-ZT13, and mice are physically removed to a cage without access to food for the remainder of the day. To control for handling, mice in FA and NA conditions are also physically moved between cages at ZT1 and ZT13. We observed that both conditions with adlib access to food (FA and NA) consumed more kcal on average than mice in the FT condition (**Fig 3a**). Given that the mice in all three conditions are unable to produce adequate amounts of insulin in fasting and fed conditions, their insulin-targeted tissues are not effectively able to take up glucose as an energy source. This may result in animals having excess hunger, and as a result, greater food consumption if given the opportunity for adlib access. Thus, we hypothesize that FA and NA mice consume more kcal than the FT mice due to this hunger and their having unlimited access to food. Although NA mice consume more kcal than the FA and FT mice, they have significantly lower weight gain. Again, this is possibly because the FT and FA mice can gain weight from the elevated amounts of fat components in their chow, which do not require insulin for uptake into storage sites. FT and FA conditions do not have significantly different body weight gain from each other over the duration of the experiment (other than on week 6 after wean) (**Fig 3b**).

Low serum insulin concentration in combination with high serum glucose concentration at the time of sacrifice confirms successful streptozotocin injections were achieved across all three conditions (**Fib 3c, Fig 3d**). Notably, the NA condition has significantly higher serum glucose concentration than the FA and FT conditions at the time of sacrifice (**Fig 3d)**. This is likely due to the fact that the composition of NCD (Teklad Diet LM-48) is 44% kcal carbohydrates, versus HFD (Research Diets, D12492i), which is only 20% kcal carbohydrates.

As expected, the FA condition develops NASH, and the NA condition does not (**Fig 3e**). Surprisingly, TRF did not protect against STAM/HFD-induced NASH (**Fig 3e**). FA and FT conditions have over 50% of mice with histological scoring of NAFLD activity Score (NAS) of 3 or greater, whereas 100% of mice in the NA condition have a NAS score of 2 or lower (**Fig 3e**).

Importantly, NAS scores of 2 or less are largely considered not diagnostic of NASH [64]. Further, 50% or more of mice in the FA and FT conditions develop fibrosis, whereas NA mice do not (**Fig 3f**). Fibrosis, which requires repeated attempts at wound healing, is an important marker of liver injury and disease progression. Natural history studies in human populations demonstrate that the severity of fibrosis is the sole histological measure that can independently predict hepatology-related morbidity (e.g., liver-related illness, liver transplantation) and mortality in individuals with NAFLD [65].

Although TRF does not protect against STAM/HFD-induced NASH, the remainder of our experiments aimed to elucidate critical information about how circadian dyssynchrony contributes to NASH in the FA condition, and what blocks TRF from preventing NASH in the STAM/HFD model. This information will provide valuable insight to new discoveries on the disease mechanisms of NASH.

2.3. STAM/HFD-Induced NASH Does Not Disrupt Feeding Rhythms

To investigate the effects of STAM/HFD-induced NASH on behavioral rhythms such as food consumption patterns and energy expenditure, mice were individually housed in metabolic cages that are capable of continuously measuring animal weight, food consumption, total daily movement, and energy expenditure. Surprisingly, despite the consumption of HFD, FA mice maintain rhythmic food consumption patterns (**Fig 4a, S1a**) and consume the same percentage of food in the dark phase as NA mice (**Fig 4b, S1b**). Additionally, FA mice have a maintenance of energy expenditure rhythms (**Fig 4c, S1c**).

2.4. Mice with STAM/HFD-Induced NASH on Adlib Feeding Have Disrupted Diurnal Fluctuations in Stool Microbiota Composition

Food consumption patterns are one of the strongest drivers of diurnal fluctuation in gut microbiome composition. Due to the surprising finding that FA mice have a maintenance of

rhythmic food consumption patterns, we wanted to investigate whether FA mice have normal diurnal fluctuations in gut microbiota composition. To accomplish this, two time point stool collections (ZT1 and ZT13) were completed at week 8 (pre-NASH development) and week 12 (NASH development) (**Chapter 1, Fig 2**) to measure diurnal changes in gut microbiota composition (16S sequencing). Although previous research indicates that mice with STAM/HFD-induced NASH have abnormal gut microbiome composition [14], the effects of STAM/HFD-induced NASH on diurnal fluctuations in gut microbiome composition have never been characterized.

Overall, the global composition of the stool microbiome is driven by diet type (weighted UniFrac Principal Coordinates Analysis) (**Fig 5a**). PC1 accounts for the greatest amount of variance in the data, and is correlated with diet type: there is no overlap seen between samples from NA vs FA and FT mice. Although there is substantial overlap between FA and FT mice, FT mice have a higher degree of separation between samples collected at ZT1 vs ZT13 along PC2. Similarly, NA mice have clear separation between ZT1 and ZT13 microbiota composition along PC2. Compared to condition and time of sample collection, disease stage at the time of sample collection is a weaker driver of global stool microbiome composition. There are no significant between-group differences in Pre-NASH vs NASH samples for any of the three conditions (weighted UniFrac PERMANOVA, $p < 0.05$). There were not significant differences in stool microbiome species richness (Faith's PD) between ZT1 and ZT13 across conditions before or during NASH (**S2a**). However, at the time of NASH onset, FT and NA conditions have greater differences in species richness between ZT1 and ZT13 than FA mice (**S2a**).

To investigate diurnal fluctuations in stool microbiome composition, we measured differences in weighted UniFrac beta diversity between ZT1 and ZT13 for each condition (**Fig 5b, Fig 5c**). Surprisingly, despite having a maintenance of food consumption patterns (**Fig 4a**, **Fig 4b**), which is a strong driver of diurnal gut microbiome rhythms, FA mice have disruptions to diurnal fluctuations in stool microbiome composition between ZT1 and ZT13 before (**Fig 5b**) and

at the time of NASH onset (**Fig 5c**). In contrast, NA mice have significant differences in stool microbiome composition between ZT1 and ZT13 before (**Fig 5b**) and during NASH onset (**Fig 5c**), as measured by significant differences in weighted UniFrac beta diversity. Similarly, FT mice also have significant differences in stool microbiome composition between ZT1 and ZT13 before and during NASH onset (**Fib 5b, Fig 5c**). Overall, our results show that diurnal changes in stool microbiome composition are disrupted before and during the onset of STAM/HFD-induced NASH. Although TRF is capable of restoring diurnal fluctuations, this restoration is not sufficient to prevent the development of NASH.

2.5. Mice with STAM/HFD-Induced NASH on Adlib Feeding Have Disrupted Diurnal Fluctuations in Ileal Microbiota Composition

In addition to quantifying diurnal changes in stool microbiome composition, which is most closely associated with the large intestine microbiome, we next quantified diurnal changes in ileum microbiome composition. The ileum plays a critical role in metabolic and immune processes that affect the function of both the gastrointestinal environment and the host systemically. For example, the ileum has high expression of the bile acid receptors farnesoid X receptor (FXR) and G protein-coupled bile acid receptor 1 (TGR5), which have various far-reaching effects on metabolism and immune processes (**Chapter 1, Table 1**). Additionally, previous studies demonstrate that diurnal rhythms in the small intestine microbiome are essential for the maintenance of barrier function and immune homeostasis in the gastrointestinal tract [66]. Our previous research indicates that HFD-induced obesity dampens diurnal rhythms of the ileal microbiome and transcriptome [55]. However, the effects of STAM/HFD-induced NASH on diurnal changes in ileal microbiome composition remain unknown.

To measure diurnal changes in ileum microbiome composition, ileal tissue (with ileal contents) was harvested at two time points (ZT1 and ZT13) at the time of NASH onset (**Chapter 1, Fig 2**). Global ileal microbiome composition is most strongly driven by condition (i.e., diet type + feeding pattern) (**Fig 6a**). All three conditions have significantly different weighted UniFrac

beta diversity (**Fig 6a**). PC1 accounts for variance in the data that can be attributed to condition, with PC3 resolving the clear separation in FA and FT conditions.

Overall, diurnal fluctuations in ileum microbiome composition followed the same patterns as stool microbiome composition (**Fig 6b**). FA mice have disruptions to diurnal fluctuations in ileum microbiota composition between ZT1 and ZT13, whereas NA mice do not (**Fig 6b**). FT mice have slightly disrupted fluctuations in ileum microbiome composition, but clear separation in weighted UniFrac beta diversity for samples collected at ZT1 vs ZT13, suggesting that these differences are trending towards significance. In contrast to the stool microbiome, NA mice have significantly higher species richness (Faith's PD) in the ileum than FA and FT mice (**Fig S3a**), which is consistent with previous studies in our lab [55].

2.6. Mice with STAM/HFD-Induced NASH Have Disrupted Diurnal Fluctuations in Stool Metabolome

The gut microbiota exerts its effects on the gut and extraintestinal organs through the modulation and production of numerous microbially-derived metabolites. Thus, disruption to diurnal changes in gut microbiome composition can result in disruptions to the gut microbial metabolome [67]. In contrast to 16S sequencing, which provides information about the taxonomic composition of the microbiome, metabolomic profiling provides direct information on the functional activity and products of the gut microbiome. Thus, investigating the gut microbial metabolome of mice with STAM/HFD-induced NASH can help us gain a mechanistic understanding of how disruptions to diurnal changes in gut microbiome composition affect disease pathogenesis through the modulation of bacterially-produced metabolites. To accomplish this, we completed untargeted metabolomics on stool collected at the same time as samples analyzed in **Fig 5**. Overall, the global composition of the stool metabolome is driven by condition (**Fig 7a**): there are significant differences between the stool metabolome of all three conditions as measured by Bray Curtis beta diversity. To quantify the diurnal shifts in the stool

metabolome, we identified the proportion of significantly increased and decreased features at ZT13 pre-NASH (**Fig 7b**), and during NASH onset (**Fig 7c**).

Pre-NASH onset, the magnitude of diurnal shifts in the stool metabolome between ZT1 and ZT13 are disrupted in FA and FT conditions (**Fig 7b**). Compared to the NA condition, FA and FT mice have a greater proportion of metabolites decreased at ZT13 (FA= 22.9%, FT= 16.9%, NA= 2.7%) (**Fig 7b**). Interestingly, ~20% of the metabolites significantly decreased in FA and FT mice are the same in both conditions (**Fig S4b**). In contrast, mice in the NA condition have very few metabolites decreased at ZT13, but rather, a greater proportion of features increased at ZT13 (FA= 0.4%, FT= 10.6%, NA= 13.5%) (**Fig 7b**). Similarly, at the time of NASH onset, FA and FT mice have a greater proportion of metabolites decreased at ZT13 than NA mice (FA= 8.7%, FT= 9.0%, NA= 7.6%), although this difference is more modest than Pre-NASH (**Fig 7c**). Further, the greatest discrepancy between conditions that develop NASH (FA and FT mice) vs those that don't (NA mice), is in the proportion of metabolites that are increased at ZT13 (FA= 2.3%, FT= 4.7%, NA= 14.8%) (**Fig 7c**). Additionally, NA mice have a greater diversity of metabolites (alpha diversity, as measured by the Shannon Index) than FA and FT mice Pre-NASH and at the time of NASH onset, (**S4a**).

The differences in the proportion of metabolites significantly increased during the ZT13 phase in FA and FT mice in comparison to NA mice suggests that disrupted fluctuation of these metabolites may be associated with disease. Thus, we next characterized the molecular subclass assignment and fold change differences of metabolites that are significantly increased at ZT13 in NA mice Pre-NASH (**Fig 7d**) and during NASH (**Fig 7e**) across all three conditions. Pre-NASH and at the time of NASH onset, the top two most abundant subclasses of metabolites that are significantly increased at ZT13 in NA mice are 1) bile acid, alcohols, and derivatives, 2) amino acids, peptides, and analogues (**Fig 7d, Fig 7e**). Next, we investigated the ZT13/ZT1 fold change of the features in these two subclasses across all conditions to determine if the

fluctuations of these metabolites are different in mice that develop NASH (FA and FT conditions) vs mice that do not (NA condition) (**Fig 7d, Fig 7e**). Pre-NASH and at the time of NASH onset, FA and FT conditions have significantly lower fold change of these metabolites compared to NA mice. This suggests that stool metabolome fluctuations that are occurring in NA mice (don't develop NASH) are disrupted in FA and FT conditions (develop NASH). Interestingly, pre-NASH, the fold changes of these metabolites are significantly different between FA and FT conditions, whereas at the time of NASH onset they are not. This suggests that pre-NASH, differences in the fluctuation of these metabolites in HFD-consuming conditions may be driven by feeding pattern (adlib vs TRF) whereas at the time of NASH onset, the similarly in the fluctuation of these metabolites may be driven by the manifestation of NASH pathology.

2.7. Discussion

Our results demonstrate that TRF is not capable of protecting against STAM/HFD-induced NASH, and that STAM/HFD mice with adlib access to food maintain rhythmic food consumption patterns. It is important to note that previous studies in our lab, as well as published studies from other research groups, have found TRF to protect against precursors of NASH, (e.g., hepatic steatosis and liver damage) in murine models that develop diet-induced obesity and insulin resistance [6,16]. Further, previous studies demonstrate that consumption of a HFD completely eliminates 24hr feeding patterns in murine models of diet-induced obesity that develop insulin resistance [6,68]. However, STAM-injected mice are hypoinsulinemic and do not become obese. Therefore, the requirement of insulin in mediating the protective effects of TRF warrants further investigation. To our knowledge, the effect of HFD on 24hr feeding patterns has never been investigated in murine models that do not develop insulin resistance. Thus, the requirement of insulin in mediating the disruptive effects of HFD on 24hr feeding rhythms requires further investigation.

Overall, our results show that diurnal fluctuations in stool and ileal microbiome composition between ZT1 and ZT13 are disrupted in STAM/HFD mice with adlib access to food (FA condition) (**Fig 5, Fig 6**). This suggests that although FA mice have a maintenance of rhythmic feeding patterns (**Fig 4 a**), even as little as 25% of HFD consumption in the light phase (**Fig 4b**) may be enough to disrupt diurnal fluctuations in stool and ileum microbiome composition. This may explain why FT mice have a robust maintenance of diurnal fluctuations in stool and ileum microbiome composition between ZT1 and ZT13, as they consume 0% of their HFD food during the light phase. Further research is needed to elucidate the mechanisms driving differences in the diurnal fluctuation of ileum and stool microbiome composition in FT and FA mice despite the overall maintenance of feeding patterns and manifestation of NASH liver pathology in both conditions.

Interestingly, we found that both FA and FT conditions have disruptions to diurnal shifts in stool metabolome between ZT1 and ZT13, despite the fact these conditions had different trends in disrupted fluctuations of gut microbiome composition. Overall, our results suggest that disruptions to the magnitude diurnal shifts in the stool metabolome between ZT1 and ZT13 track wtih disease progression (**Fig 7a, Fig 7b**). Additionally, we find that in mice that develop NASH (FA and FT conditions) there are disrupted fluctuations of metabolites that are significantly increased at ZT13 in the NA condition, suggesting that these metabolites may play a role in driving STAM/HFD-induced NASH pathogenesis. The top two molecular subclasses of features that are significantly increased in NA mice at ZT13 are 1) bile acid, alcohols, and derivatives, and 2) amino acids, peptides, and analogues (**Fig 7d,e**). Previous research demonstrates that these molecular subclasses play crucial roles in NASH pathogenesis.

BA homeostasis is dysregulated during NASH [58,59]. For example, compared to healthy controls, patients with NASH have higher levels of total fecal BAs, CA, chenodeoxy cholic acid, and BA synthesis, and an increased ratio of primary to secondary fecal BAs [58]. In

a study of individuals with biopsy-proven NAFLD, total unconjugated serum BAs were lower in individuals with NASH and fibrosis, and total serum BAs are elevated during fibrosis, when compared to individuals with NAFLD [59]. Dysregulation of BA homeostasis during NASH can affect disease pathophysiology via dysregulation of host metabolic processes that are modulated by the BA receptors FXR and TGR5 (**Chapter 1, Table 1**). Disruptions in BA homeostasis may perturb these metabolic processes via deregulation of their receptors. The expression of the BA receptors *Fxr* and *Tgr5* are down-regulated during NASH [60]. Overall, these findings suggest that NASH may promote a luminal environment with a greater proportion of BAs that function as FXR and TGR5 antagonists.

Additionally, gut microbially-derived metabolites resulting from the metabolism of the amino acids are also implicated in NASH pathogenesis [67]. For example, tryptophan metabolism is disrupted during NASH. Studies demonstrate that changes in gut microbiome composition during NASH are associated with tryptophan dysmetabolism, resulting in dysregulated metabolism of tryptophan's downstream metabolites such as indole and kynurenine [67]. Indole is decreased during NASH, which results in increased inflammation, decreased gut barrier function, and decreased lipogenesis. Additionally, the kynurenine pathway is overactivated during NASH, which increases inflammation. The amino acid phenylalanine and its derivative phenylacetic acid are also implicated in NASH pathogenesis. Previous human microbiome metagenomic and metabolomic studies demonstrate that hepatic steatosis is associated with increased abundance of phenylacetic acid production, as well as microbial gene pathways that promote its synthesis [69]. This result is supported in murine studies, where chronic phenylacetic acid administration is associated with hepatic steatosis.

It is important to note that since our results measuring changes to the gut microbiome and metabolome have two collection time points over a 24hr period, it is not possible to ascertain whether there are rhythmic changes that ultimately increase or decrease the

amplitude or phase of cycling for the microbes and metabolites being investigated. Two time point collections are able to capture differences seen between ZT1 and ZT13, and compare how these differences vary across each condition. However, since conditions may be phase-shifted in relation to each other, it's impossible to know whether these two time points are capturing the maximum amplitude of observed differences over a 24hr period. For example, the greater differences seen in the ZT13/ZT1 fold change of bile acid and amino acid metabolites in the NA condition relative to the FA and FT conditions (**Fig 7**) may be the result of FA and FT mice being phase-shifted, or having different amplitudes, related to NA mice. Thus, our overall conclusions drawn from this data show that there are 1) disruptions to diurnal fluctuations in gut microbiome composition between ZT1 and ZT13 for STAM/HFD mice with adlib access to food, and 2) disruptions to diurnal fluctuations in gut microbial metabolome between ZT1 and ZT13 for mice that develop NASH (FA and FT conditions) compared to mice that don't (NA condition). However, our results cannot determine the definitive rhythmic changes (e.g., amplitude or hours phase shifted) of circadian disruptions.

2.8. Research Methods

2.8.a. Experimental Methods

Animal Model: The streptozotocin (STAM) + high-fat diet (HFD) murine model of NASH was used for this study [7]. C57BL/6 male mice were injected with 0.2 mg of STAM (Cayman chemical item no. 13104) per day for five consecutive days starting at 10-12 days after birth. Male mice born within a week of each other were considered as a single cohort for the study. Mice were housed three to a cage, with each mouse coming from a different dam to prevent pre-wean cage effects that could bias the data. Only male mice were used for the experiment because female STAM/HFD mice do not develop NASH. At 4-5 weeks of age (post-wean), hyperglycemia (>200 mg/dl) was confirmed by colorimetric urinalysis strips [70]. After hyperglycemia was confirmed, mice were maintained on a high-fat diet (60% kcal fat, Research

Diets, D12492i) or normal chow diet (Teklad Diet LM-48) depending on condition assignment for the duration of the study (see “Feeding Pattern Manipulation” below for conditions).

Weight and Food Intake: Individual animal weights and cage-averaged food intake were measured once per week following weaning at the same time for the duration of the study using a standard digital scale.

Feeding Pattern Manipulation: Mice were maintained on a 12-hour light (ZT0-12) 12-hour dark (ZT12-24) light cycle. Mice either had *ad libitum* (adlib) access to food, or time-restricted access to food from ZT13-21 (TRF). From ZT13-21, mice in the TRF group were physically moved from a cage without food to a cage with access to food. Mice with adlib access to food were also moved between cages at the same times as the TRF group to control for handling. For this study, we used 12 mice in each of the 3 conditions (36 mice total): 1) STAM + HFD + adlib access to food (FA), 2) STAM + normal chow diet (NCD) + adlib access to food (NA) and, 3) STAM + HFD + TRF access to food from ZT13-ZT21 (FT).

Fecal Collection: Prior to starting a high-fat diet, we collected a single time point stool sample from all mice to rule out founder effects in our microbiome research. Two time point stool was collected from mice before NASH pathology (8 weeks) and at the time of NASH onset (12 weeks) at ZT1 (light phase) and ZT13 (dark phase) to quantify diurnal changes in gut microbiome composition. For the experiment, we used a subset of 6 mice in each of the 3 conditions. Every mouse came from a different home cage, as each individual cage is only considered as an n=1 for microbiome characterization. Single-housed mice were placed in clean cups at ZT1 and ZT13, and a minimum of 3 pellets of fresh stool were collected at each time point before returning mice to their home cage. Stool was stored at -80°C and later processed for 16S rRNA gene amplicon (16S) sequencing and untargeted metabolomics.

Metabolic Cage Phenotyping: At 13 weeks old, a separate cohort of mice underwent metabolic cage phenotyping (FA and NA, n=3/condition, FT, n=8). Single housed mice were placed in Promethion metabolic cages that are capable of continuously measuring animal

weight, food consumption, total daily movement, wheel running activity, and respiratory exchange rate (RER) [71]. Animals underwent metabolic cage phenotyping for five days total, with 2 days allotted at the start of the experiment for cage acclimation.

Sacrifice: Mice were sacrificed at the time of NASH onset (week 12). A two time point sacrifice was completed at ZT1 and ZT13, with half of the mice in each condition sacrificed at each timepoint. Prior to euthanasia, a submandibular bleed was completed to collect blood for serum insulin and glucose quantification (see "Serum Insulin and Glucose Quantification" below). Liver and ileum tissue was harvested at the time of sacrifice. A section of the right medial lobe was harvested for liver histology, and a section of the left medial lobe was harvested for transcriptomics analysis (**Chapter 3**). Liver and ileum tissue samples for RNA-sequencing analysis (**Chapter 3**) were flash frozen in liquid nitrogen and then stored at -80℃.

Histology: Prior to histological preparation, photos were taken to catalog macroscopic liver appearance. Next, a section of the right medial lobe was placed in 4% paraformaldehyde until being sectioned for histology. Liver sections underwent H & E (hematoxylin and eosin) and sirius red staining. Histological features were scored by a pathologist using the NAFLD activity score (NAS), a semi-quantitative scoring system which quantifies the extent of steatosis (0-3), lobular inflammation (0-3), and hepatocellular ballooning (0-2).

16S Sample Extraction: For stool samples, DNA extraction was completed using the Earth Microbiome Project 16S Illumina Amplicon Protocol [72,73]. For ileum samples, a total nucleic acid extraction was completed using MagMAX Microbiome Ultra (catalog #A42357) on powderized tissue (mortar and pestle on dry ice) as previously described [74] (**Chapter 3**).

LC-MS/MS Sample Extraction: flash frozen (liquid nitrogen) tissue samples were powderized (by mortar and pestle on dry ice) and stored at -80°C until extraction. At the time of extraction, samples were thawed on ice, weighed, and a clean/sterile stainless steel bead was added to each sample. Extraction was performed with 50% MeOH/water (10-20 µL of solvent

were added for each 1 mg of sample), samples were homogenized at 25 Hz for 5 min, then centrifuged at max speed for 15 min. Supernatants were concentrated using a centrifugal low pressure system then stored at -80°C once dry. Samples were reconstituted using reconstitution solvent (80% MeOH/20% water + 1µM sulfadimethoxine), centrifuged, and supernatant was removed for analysis.

LC-MS/MS Data Acquisition: 5 µL were injected into a Vanquish UHPLC system coupled to a Q-Exactive orbitrap mass spectrometer (Thermo Fisher Scientific, Bremen, Germany). For the chromatographic separation, a C18 porous core column (Kinetex C18, 150 x 2 mm, 1.8 um particle size, 100 A pore size, Phenomenex, Torrance, USA) was used. For gradient elution, a high-pressure binary gradient system was used. The mobile phase consisted of solvent A H2O + 0.1 % formic acid (FA) and solvent B acetonitrile (ACN) + 0.1 % FA, unless otherwise specified. The flow rate was set to 0.5 mL/min, unless otherwise specified. After injection, the samples were eluted with the following linear gradient: 0-1 min, 5% B, 1-4 min 5-60% B, 4-10 min 60-99%, followed by a 3 min washout phase at 99% B and a 3 min re-equilibration phase at 5% B. Data-dependent acquisition (DDA) of MS/MS spectra was performed in positive mode. Electrospray ionization (ESI) parameters were set to 53 L/min sheath gas flow, 14 L/min auxiliary gas flow, 0 L/min sweep gas flow, and 400°C auxiliary gas temperature; the spray voltage was set to 3.5 kV and the inlet capillary to 320°C and 50 V S-lens level was applied. MS scan range was set to 150-1500 m/z with a resolution at m/z 200 (Rm/z 200) of 17,500 with one micro-scan. The maximum ion injection time was set to 100 ms with an automated gain control (AGC) target of 1.0E6. Up to 5 MS/MS spectra per MS1 survey scan were recorded DDA mode with Rm/z 200 of 17,500 with one micro-scan. The maximum ion injection time for MS/MS scans was set to 100 ms with an AGC target of 5E5 ions . The MS/MS precursor isolation window was set to m/z 1. The normalized collision energy was set to a stepwise increase from 20 to 30 to 40% with z = 1 as default charge state. MS/MS scans were triggered at the apex of chromatographic peaks within 2 to 15 s from their first occurrence. Dynamic precursor exclusion

was set to 5 s. Ions with unassigned charge states were excluded from MS/MS acquisition as well as isotope peaks.

Serum Insulin and Glucose Quantification: Serum insulin and glucose concentrations were calculated from serum collected at the time of sacrifice. Serum insulin was quantified using Crystal Chem's Ultra Sensitive Mouse Insulin ELISA Kit (cat. 90080). Serum glucose was quantified using Crystal Chem's Mouse Glucose Assay Kit (cat. 81692).

2.8.b. Data and Statistical Analysis

Metabolic Cage Analysis: Data was collected for 5 days, and the first two days were eliminated to account for the acclimation period. Raw file outputs from Promethion metabolic cages were converted to .xml format using MacroInterpreter software (v2.38). Data was was binned into 1 hour intervals per animal for data analysis and graphing in R Studio. Averages of each behavior (e.g., food consumption, energy expenditure) were calculated for each condition. Differences between conditions were determined using Kruskal Wallis test with FDR correction (alpha = 5%) and comparisons of area under the curve.

16S Sequencing*:* 16S rRNA sequencing was completed using the Earth Microbiome Project 16S Illumina Amplicon Protocol [72,73]. Raw sequencing data was uploaded to Qiita (https://qiita.ucsd.edu/) [75]. Raw sequences were demultiplexed, trimmed to 150, and processed using Deblur 2021.09 with default parameters on Qiita. 16S feature tables pre-processed in Qiita as described were analyzed using QIIME2 version 2022.2 [76]. After rarefying the samples to the same sequencing depth, α-diversity (within-group species diversity), β-diversity, and differential abundance analysis was performed. Ileum samples were rarefied to 4,800, resulting in 1 sample lost per condition. Stool samples were rarefied to >10,000 with 100% sample retention. α-diversity measures were compared between conditions using a pairwise Kruskal Wallis test, and corrected for multiple hypothesis testing using the FDR method. β-diversity measures were compared using pairwise PERMANOVA, which tests for

differences between group centroids for non-parametric datasets having two or more groups. Previous studies show that 3-4 mice per time point is minimally sufficient to identify changes in gut microbiome composition [5]. Thus, 6 mice per condition is more than sufficient to detect perturbations (power= 80%, alpha= 5%).

LC-MS/MS Feature Finding: An in-house modified version of MZmine2.37, corr.17.7 available at https://mzmine.github.io/iin_fbmn was utilized to perform all feature finding steps. Feature tables (csv) and MS/MS spectra files (mgf) were exported, uploaded to MassIVE, and submitted to GNPS [77] for feature-based molecular networking analysis. MS/MS spectra were converted to .mzML files using msConvert (ProteoWizard). MS1 feature extraction and MS/MS pairing were performed with MZmine. An intensity threshold of 5E4 for MS1 spectra and of 5E2 for MS/MS spectra was used. MS1 chromatogram building was performed within 10 ppm mass windows and a minimum peak intensity of 5E4. Extracted Ion Chromatograms (XICs) were deconvoluted using the local minimum search algorithm with a chromatographic threshold of 80%, a search minimum in RT range of 0.2 min, and a median m/z center calculation with m/z range for MS2 pairing of 0.01 and RT range for MS2 scan pairing of 0.2 min. MS1 feature lists were joined using an m/z tolerance of 10 ppm and retention time tolerance of 0.3 min; alignment was performed by placing a weight of 75 on m/z and 25 on retention time. Feature areas and feature correlation pairs were exported as .csv files. The corresponding consensus MS/MS spectra were exported as an .mgf file. For spectral networking and spectral library matching, all files were uploaded to the feature-based molecular networking workflow (FBMN) on GNPS (gnps.ucsd.edu) [77].

Feature Based Molecular Networking: The precursor ion mass tolerance was set to 0.01 Da and the MS/MS fragment ion tolerance to 0.01 Da. A molecular network was then created where edges were filtered to have a cosine score above 0.70 and more than 6 matched peaks. Further, edges between two nodes were kept in the network if and only if each of the nodes appeared in each other's respective top 10 most similar nodes. Finally, the maximum size of a

molecular family was set to 100, and the lowest scoring edges were removed from molecular families until the molecular family size was below this threshold. The spectra in the network were then searched against GNPS spectral libraries and NIST17. The library spectra were filtered in the same manner as the input data. All matches kept between network spectra and library spectra were required to have a score above 0.7
and at least 5 matched peaks.

Compound Class Prediction Using SIRIUS and CANOPUS: Molecular formulas were assigned using the SIRIUS GUI [78]. mgf outputs were imported into SIRIUS, and SIRIUS, CSI:FingerID, and CANOPUS [79] analyses were performed with the following parameters.

SIRIUS parameters	
Instrument	Orbitrap
Filter by isotope pattern	yes
MS/MS isotope scorer	Score
MS/MS mass accuracy	10 ppm
Candidates stored	10
Min candidates per ion	1
Use heuristic above m/z	300
Use heuristic only above m/z	650
CSI:Finger ID parameters	
Fall back adducts	all
Score threshold	yes
Search databases	all
Tag lipids	yes

Metabolomics Comparative Analysis: Metabolomics β-diversity and α-diversity were calculated using QIIME2 [76]. β-diversity measures were compared using pairwise

PERMANOVA. For volcano plots, statistical significance was assessed using a t-test (a = 5%), then corrected for multiple hypothesis testing with the FDR method. Significance thresholds for significantly increased and decreased metabolites were set at +/-1 Log2(FoldChange) and $p < 0.05$. Previous studies show that 3-4 mice per time point is minimally sufficient to identify changes in gut microbial metabolome composition [5]. Thus, 6 mice per condition is more than sufficient to detect perturbations (power= 80%, alpha= 5%).

For all other comparative analyses (e.g., animal weight and food consumption, glucose and insulin concentration, log ratio comparisons) we used a Kruskal Wallis test (alpha= 0.05) and corrected for multiple hypothesis testing using the FDR method.

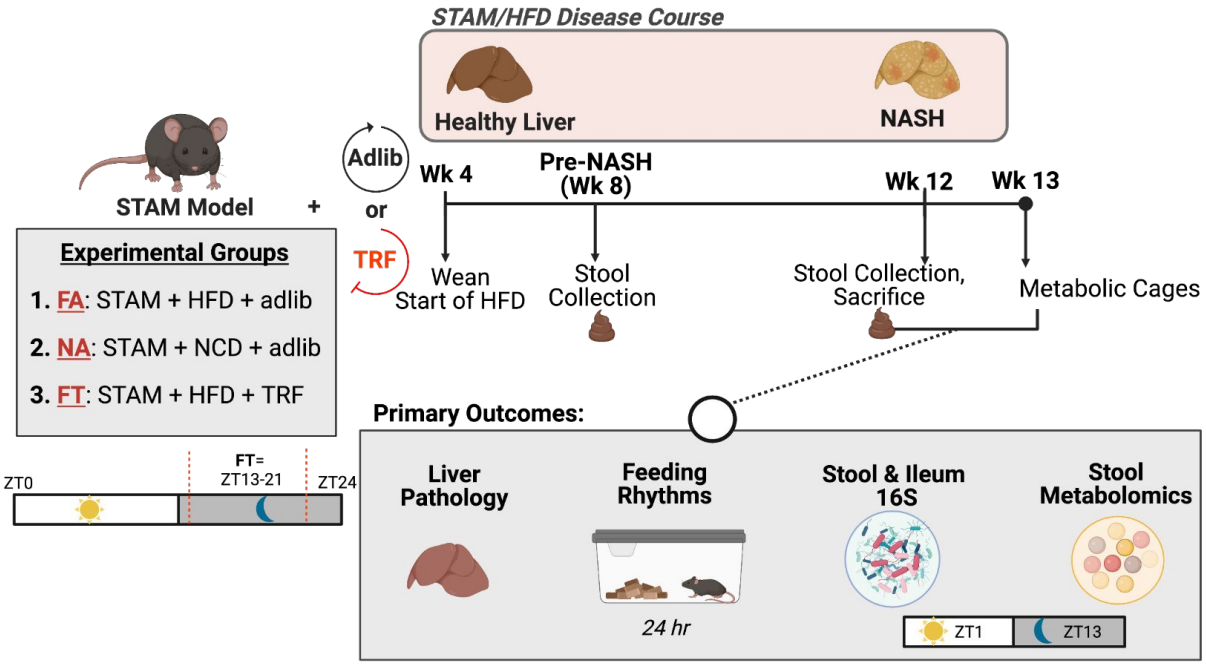

Figure 2. Experimental Design

All three experimental groups are injected with streptozotocin (STAM) during the early postnatal phase, resulting in hyperglycemia and hyperinsulinemia. FA, NA, and FT conditions (n=12/condition) vary by diet type and access to food. FA and FT mice consume high-fat diet, and NA mice consume normal chow diet. FA and NA mice had access to 24hrs/day (adlib), and FT mice had time-restricted access to food from ZT13-ZT21 (TRF) starting at 4 weeks of age. FA mice develop NASH at 12 weeks, and NA mice do not develop NASH (control). FT mice are the treatment condition. Two 2 time point stool collections (ZT1 and ZT13) were completed at week 8 (pre-NASH development) and week 12 (NASH development). A week 12, a two time point sacrifice was completed (ZT1 and ZT13) with half of each condition being sacrificed at each ZT time. Two time point stool collections and sacrifices were completed to measure diurnal gut microbiota changes (16S, metabolomics), and gene expression (liver and ileum transcriptomics) between ZT1 and ZT13. NASH liver pathology was determined via histological analysis. Successful establishment of streptozotocin model (hyperglycemia and hyperinsulinemia) was determined by immunoassay on blood serum collected at the time of sacrifice. A separate cohort of mice was used for metabolic phenotyping at week 13 (FA and NA, n=3/condition. FT, n=8.). Graphic Illustration Source: BioRender.

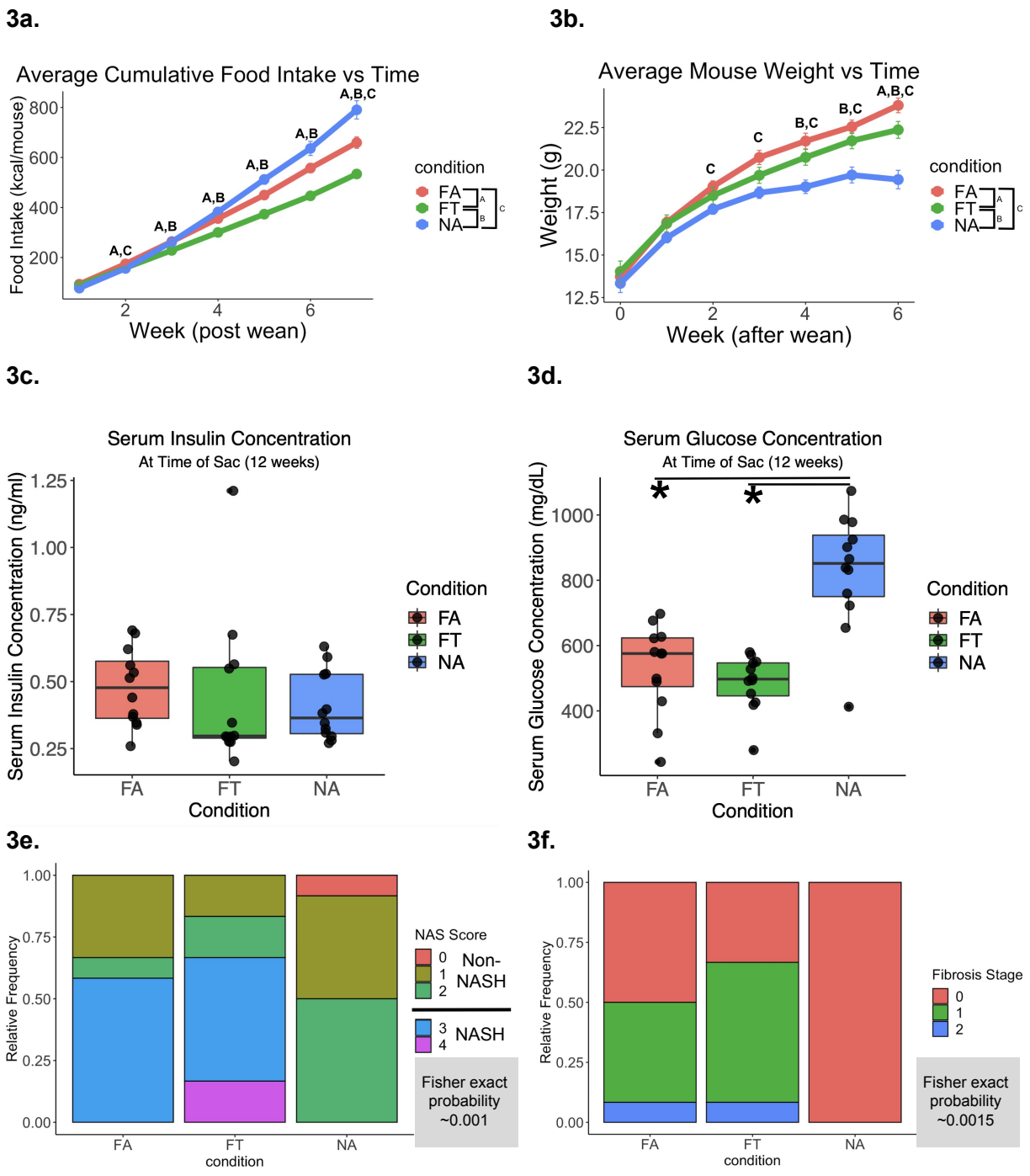

Figure 3. Time-Restricted Feeding Does Not Prevent STAM/HFD-Induced NASH
Average cumulative food intake (A) and body weight (B) per mouse per condition (n=12/condition). Low serum insulin (C) and high serum glucose concentration (D) at the time of sacrifice (12 weeks) across all three conditions confirms successful streptozotocin injections. FA and FT mice develop NASH, whereas NA mice do not (E), as measured by histology NAFLD Activity Score (NAS). (F) NA mice do not develop fibrosis. (A, B, C, * = $p < 0.05$, Pairwise Mann-Whitney U test, FDR correction)

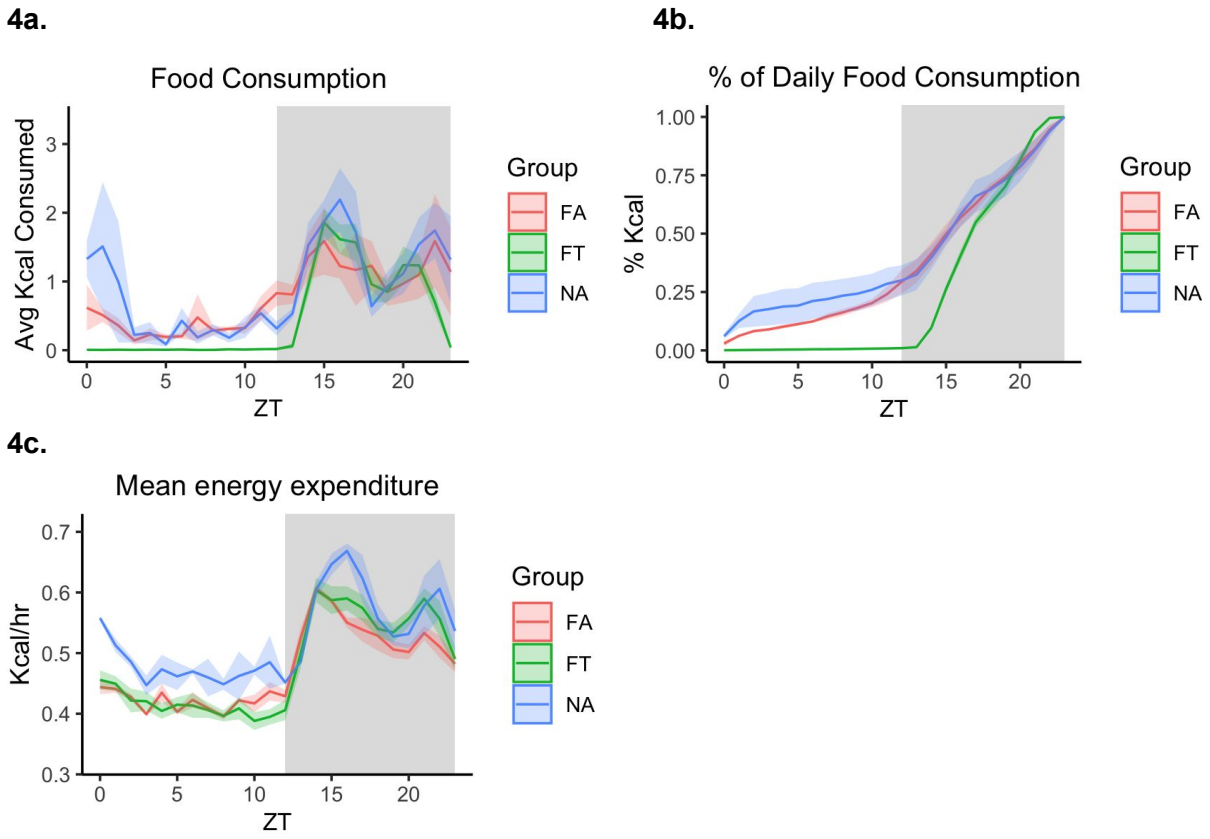

Figure 4. STAM/HFD-Induced NASH Does Not Disrupt Feeding Rhythms
Food consumption (A), percent daily food consumption (B), and mean energy expenditure (C), averaged over 72 hours in one hour bins. FA mice have a maintenance of behavioral rhythms, including food consumption and mean energy expenditure. FT mice had access to to food from ZT13-ZT21 (gray). FA and NA, n=3/condition. FT, n=8.

S1a.

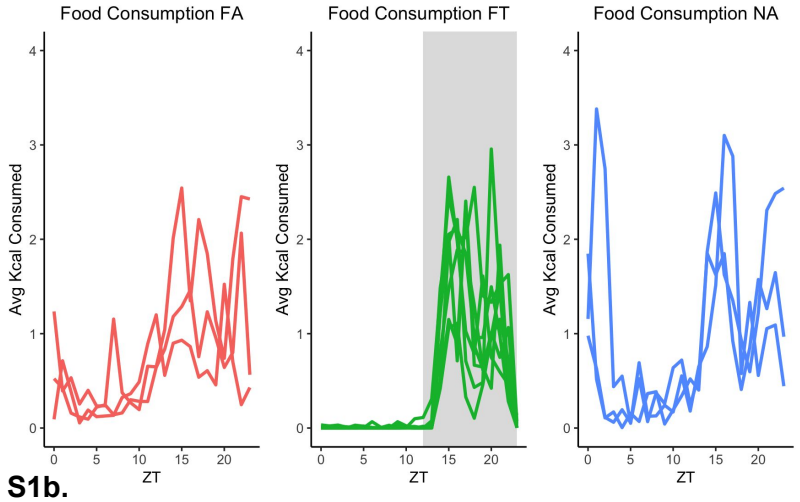

S1b.

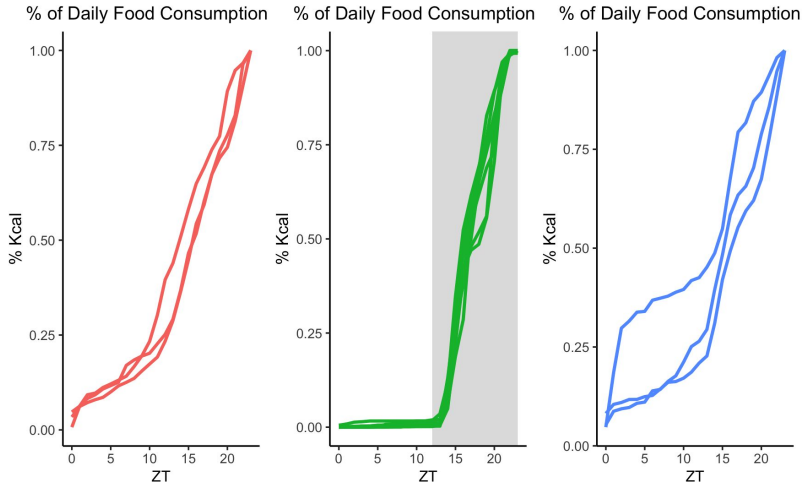

S1.c.

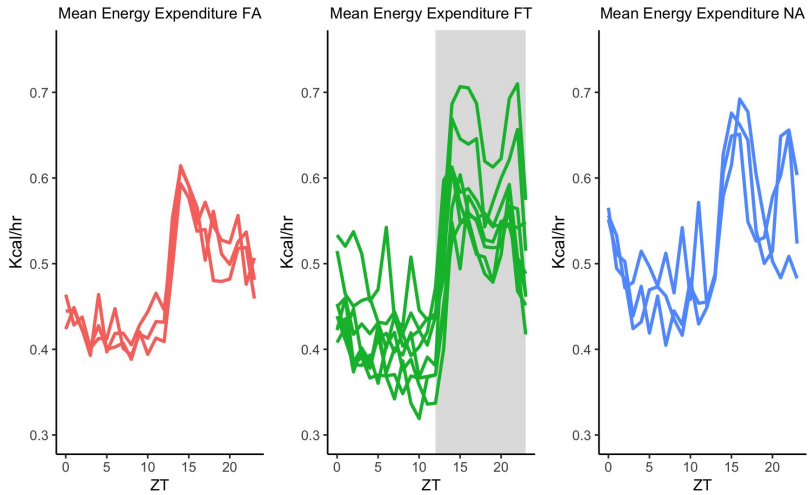

Supplemental Figure 1. Individual Animal Traces for Behavioral Rhythms
Individual recordings of food consumption (A), percent daily food consumption (B), and energy expenditure (C), for results displayed in main **Figure 4**. FA and NA, n=3/condition. FT, n=8.

5a.

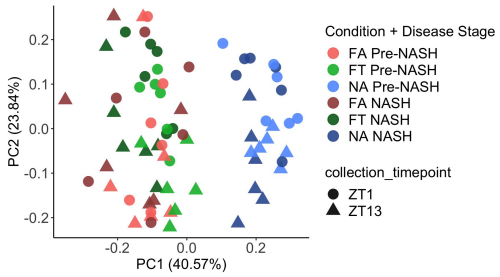

PERMANOVA	pseudo-F	pval
NA vs FA	36.65	.001
NA vs FT	42.52	.001
FA vs FT	1.52	.177

5b.

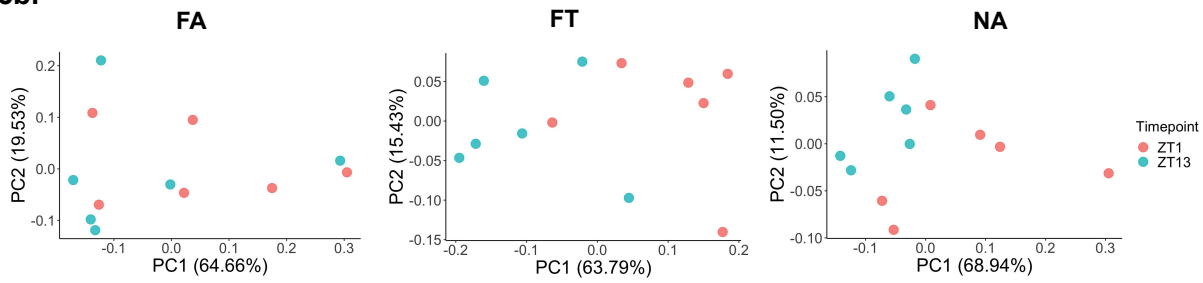

PERMANOVA	pseudo-F	pval
ZT1 vs ZT13	0.068	0.547

PERMANOVA	pseudo-F	pval
ZT1 vs ZT13	6.47	0.008

PERMANOVA	pseudo-F	pval
ZT1 vs ZT13	3.76	0.033

5c.

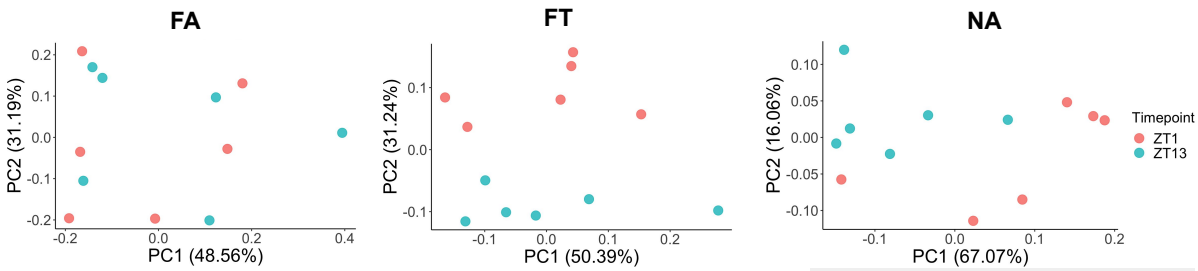

PERMANOVA	pseudo-F	pval
ZT1 vs ZT13	0.28	0.896

PERMANOVA	pseudo-F	pval
ZT1 vs ZT13	4.08	0.018

PERMANOVA	pseudo-F	pval
ZT1 vs ZT13	4.65	0.023

Figure 5. FA Results in Disrupted Diurnal Fluctuations in Stool Microbiome Composition
(A) Stool 16S weighted UniFrac beta diversity across all data (all collection time points included). Global microbiome composition is driven by diet type. (B, C) ZT1 vs ZT13 at week 8 (pre-NASH development) (B) and week 12 (NASH development) (C) per each condition (n=6 mice/condition). Despite having a maintenance of feeding pattern (Figure 4a, 4b), FA mice have disruptions to diurnal compositional changes between ZT1 and ZT13 (B, C).

S2a.

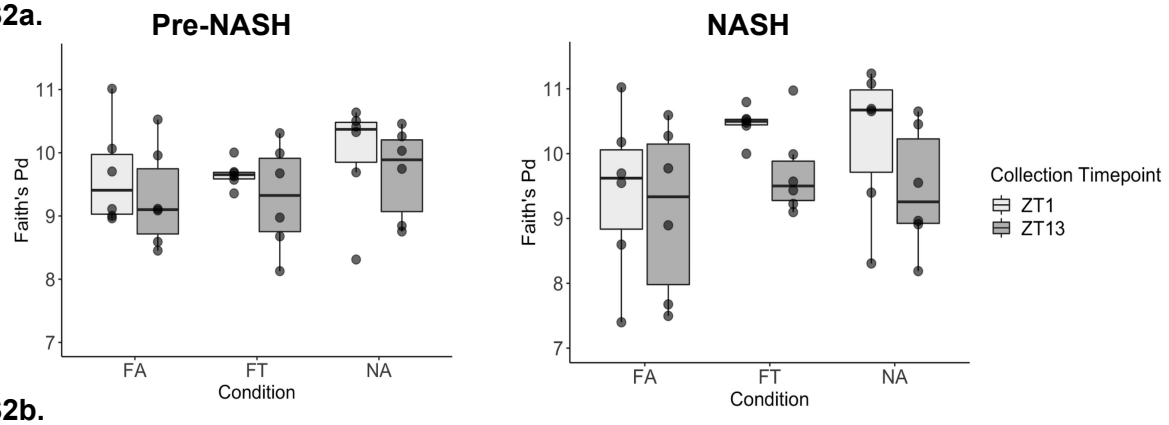

S2b.

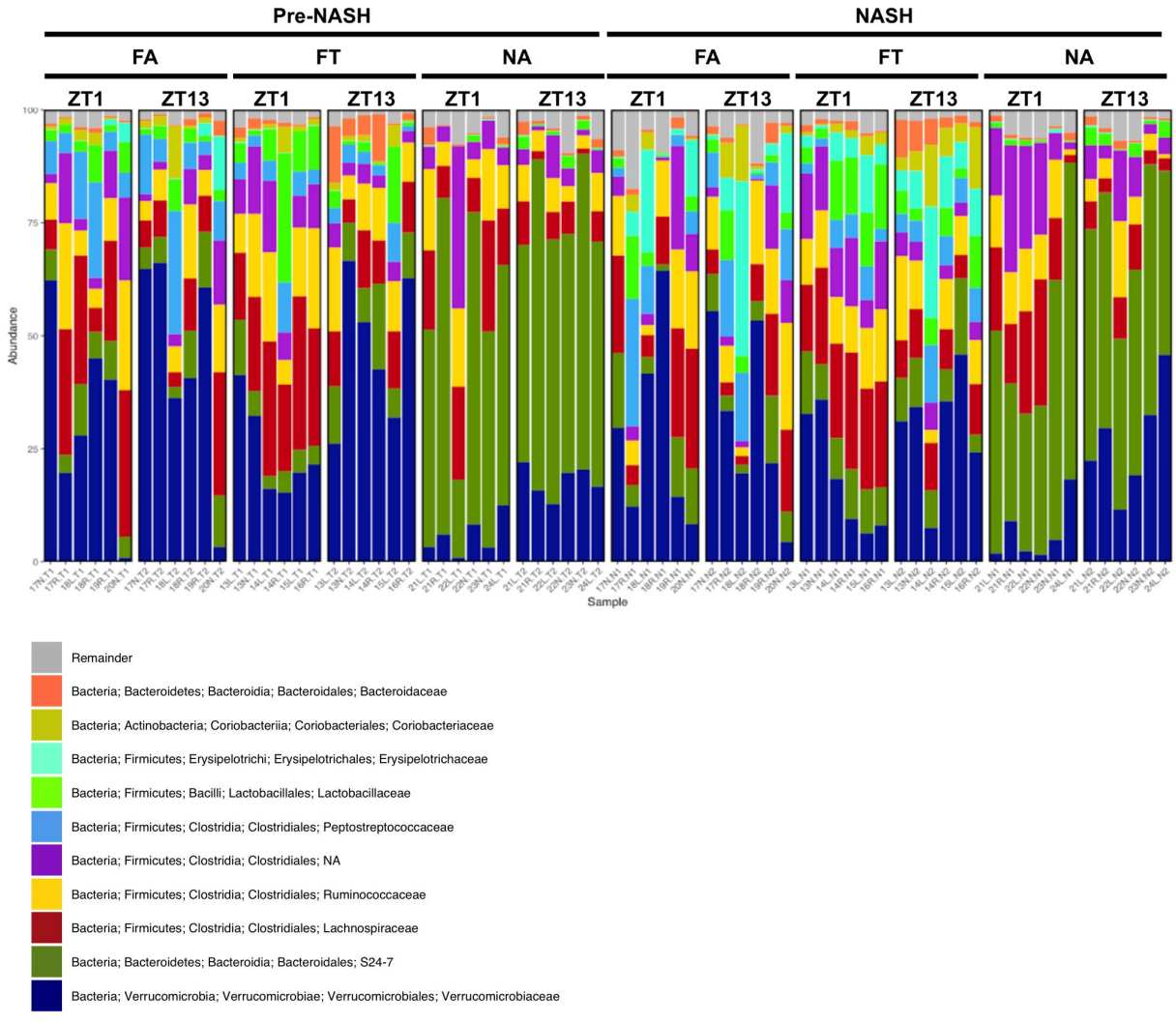

Supplemental Figure 2. Additional 16S Composition Measurements – Stool
(A) Faith's PD alpha diversity before and at the time of NASH onset (B) Relative abundance of bacterial taxa, separated by condition, ZT time, and collection disease stage.

6a. **16S: All Ileum Data**

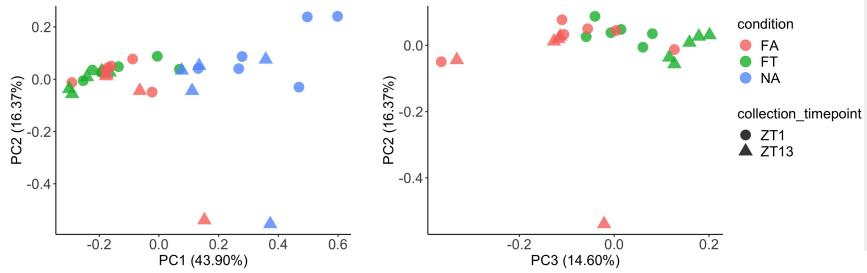

PERMANOVA	pseudo-F	pval
NA vs FA	10.54	.001
NA vs FT	13.70	.001
FA vs FT	3.66	.009

6b.

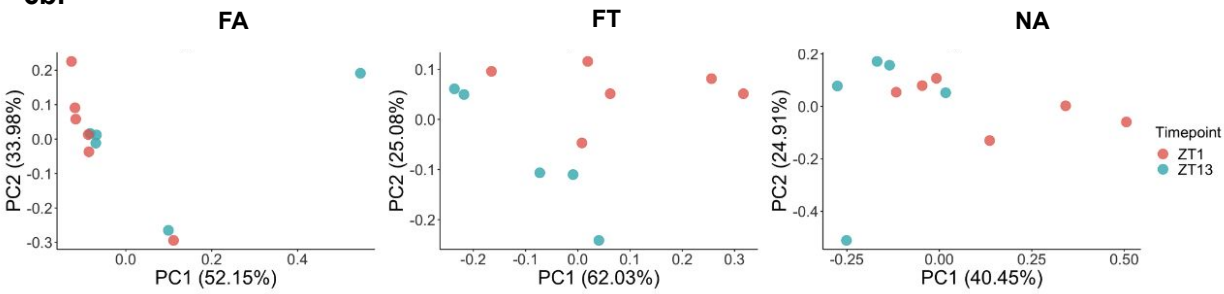

PERMANOVA	pseudo-F	pval
ZT1 vs ZT13	1.00	0.371

PERMANOVA	pseudo-F	pval
ZT1 vs ZT13	3.65	0.058

PERMANOVA	pseudo-F	pval
ZT1 vs ZT13	2.48	0.035

Figure 6. FA Results in Disrupted Diurnal Fluctuations in Ileum Microbiome Composition
(A) Ileum 16S Weighted Unifrac beta diversity across all data (all collection time points included). (B) Weighted UniFrac ZT1 vs ZT13 per each condition. Global microbiome composition is driven by condition (diet type and feeding schedule) (n=6 mice/condition). FA mice do not have compositional changes in overall ileum microbiome composition between ZT1 and ZT13.

S3a.

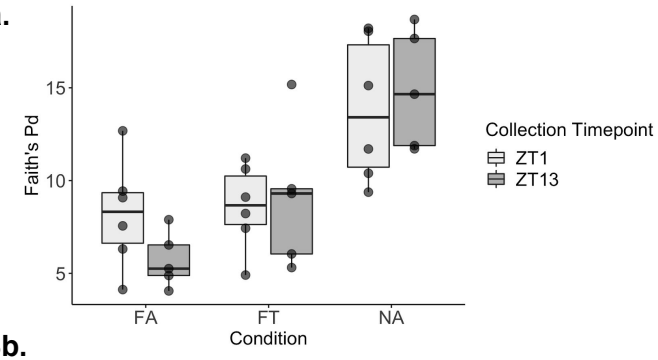

S3b.

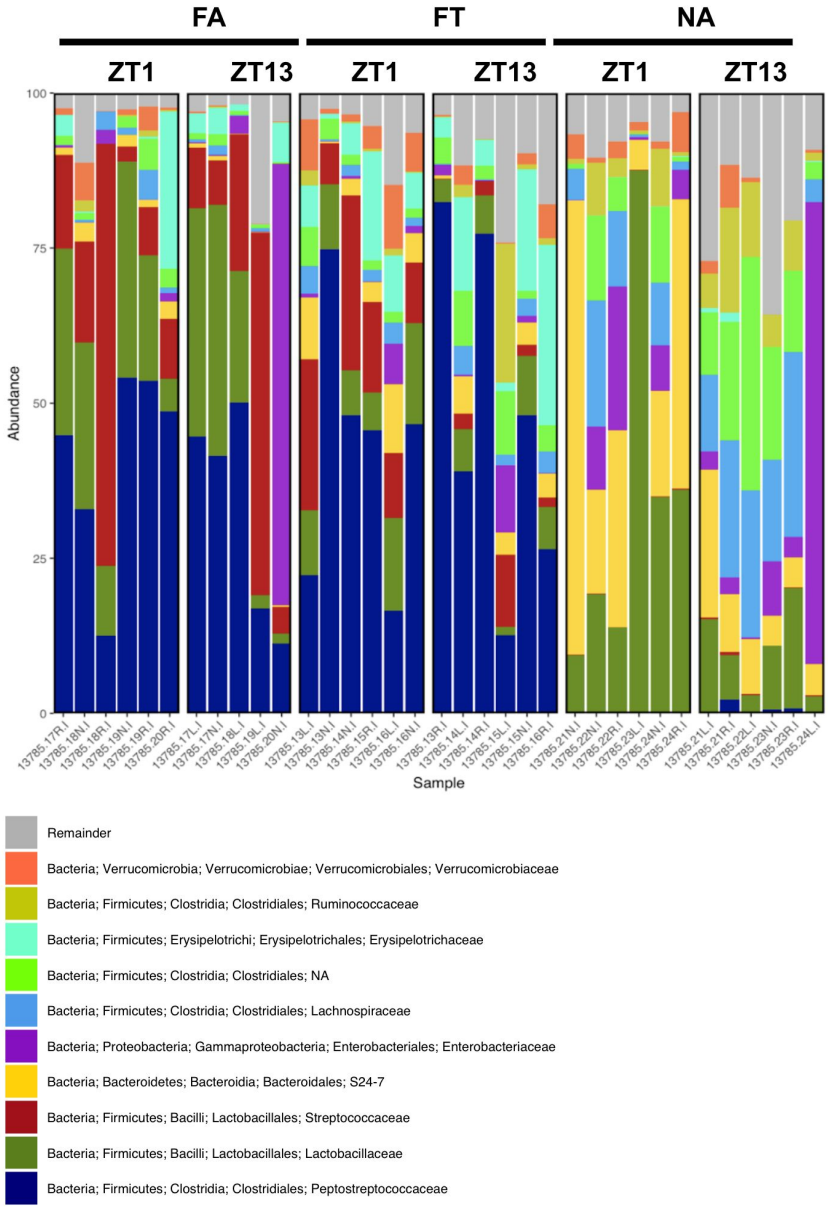

Supplemental Figure 3. Additional 16S Composition Measurements – Ileum (**A**) Faith's PD alpha diversity. (**B**) Relative abundance of bacterial taxa, separated by condition and ZT time.

Two-Paged Figure

Figure 7. STAM-Induced NASH Results in Disrupted Fluctuations in Stool Metabolome
(A) Stool metabolomics Bray Curtis beta diversity across all data (all collection time points included). Global stool metabolome composition is driven by condition (diet type and feeding schedule). (B, C) Metabolites identified as significantly increased at ZT13 (red) or significantly decreased at ZT13 (blue) at week 8 (pre-NASH development) (B) and week 12 (NASH development) (C). Significance thresholds set at +/-1 log2(FoldChange) and p-value of 0.05 (t-test, FDR correction). Tables below volcano plots indicate the proportion of metabolites within each category, per condition. (D) Pre-NASH, the molecular subclass of features identified as significantly increased at ZT13 in the NA condition. Bottom: The Log2FoldChange(ZT13/ZT1) of features identified as significantly increased in the NA condition, grouped by subclass. Top two subclasses shown. (E) As in D, but at NASH onset.
For metabolomics, n=6 mice/condition per ZT (1 or 13) per disease stage (Pre-NASH or NASH). *= $p < 0.05$ (Mann-Whitney U Test, FDR correction)

7a. **Metabolomics: All Stool Data**

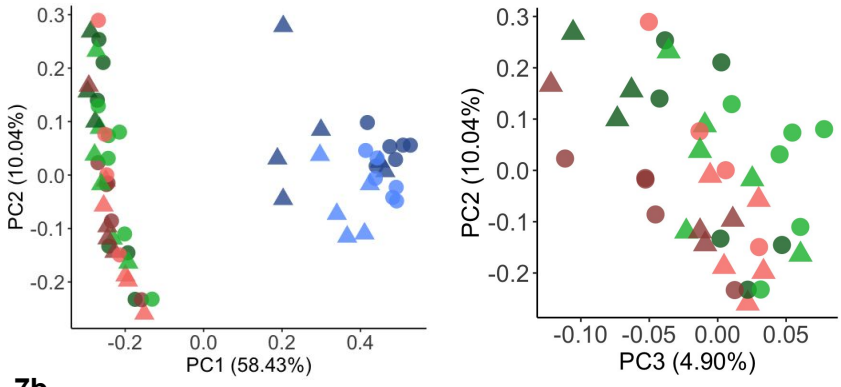

PERMANOVA	pseudo-F	pval
NA vs FA	58.58	.001
NA vs FT	57.38	.001
FA vs FT	5.12	.001

7b. **Pre-NASH**

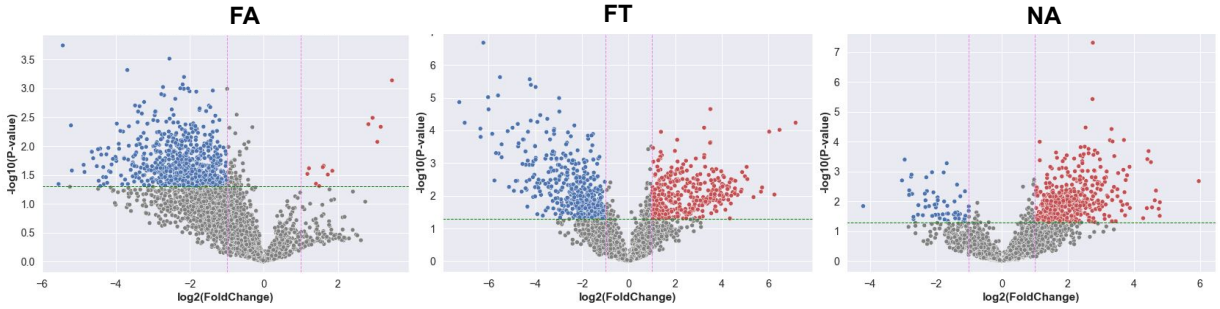

Decreased at ZT13	Same	Increased at ZT13	Decreased at ZT13	Same	Increased at ZT13	Decreased at ZT13	Same	Increased at ZT13
747 (**22.9%**)	2,509	13 (**0.4%**)	546 (**16.9%**)	2,348	342 (**10.6%**)	93 (**2.7%**)	2,849	470 (**13.5%**)

7c. **NASH**

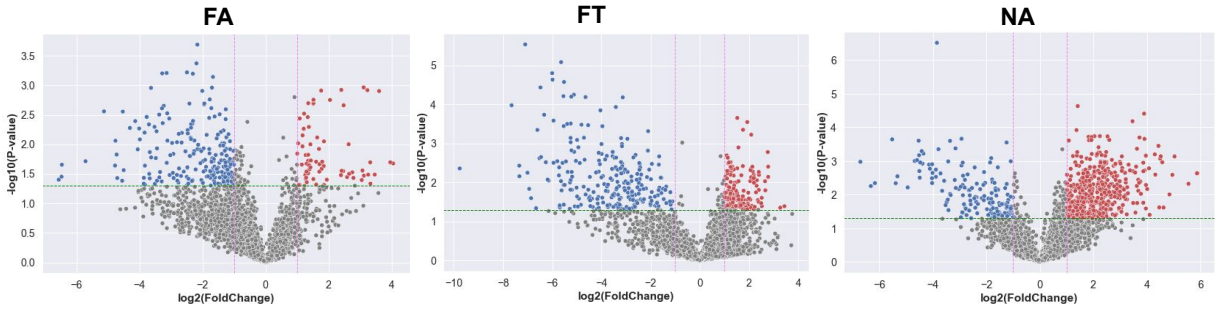

Decreased at ZT13	Same	Increased at ZT13	Decreased at ZT13	Same	Increased at ZT13	Decreased at ZT13	Same	Increased at ZT13
272 (**8.7%**)	2,787	73 (**2.3%**)	280 (**9.0%**)	2,683	147 (**4.7%**)	257 (**7.6%**)	2,621	498 (**14.8%**)

Figure 7 Page 1 of 2

7d.

Pre-NASH

Top 5 Significantly Increased at ZT13 in NA

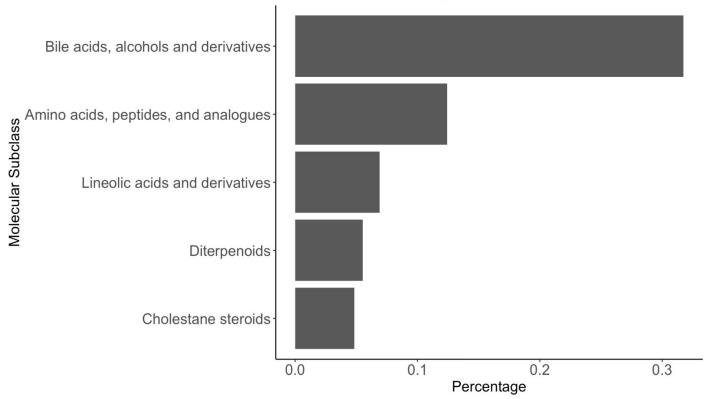

Bile acids, alcohols, & derivatives

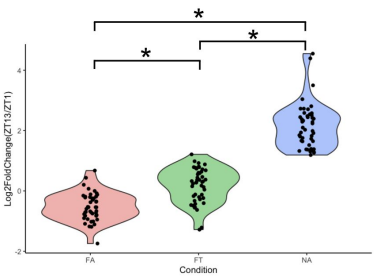

Amino acids, peptides, & analogues

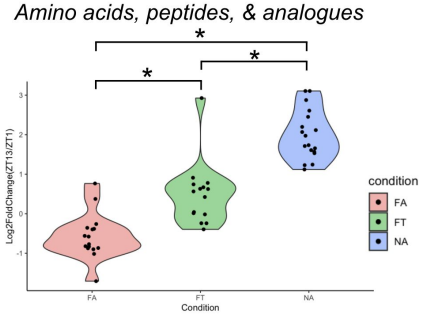

7e.

NASH

Top 5 Significantly Increased at ZT13 in NA

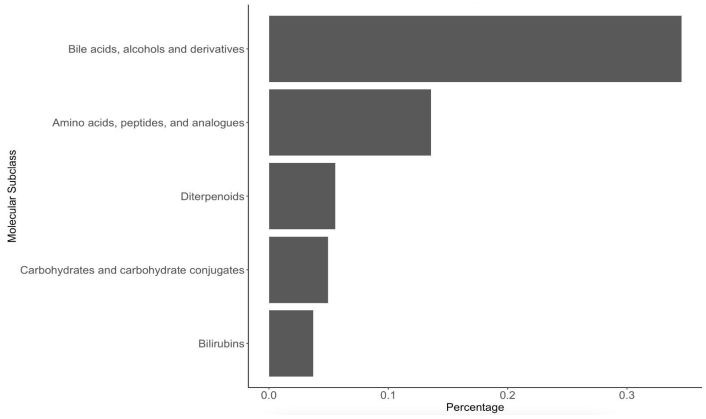

Bile acids, alcohols, & derivatives

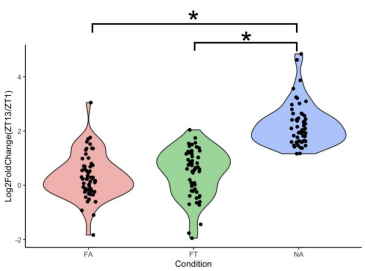

Amino acids, peptides, & analogues

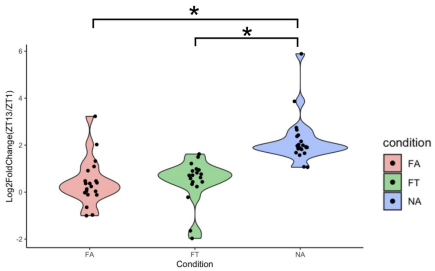

Figure 7 Page 2 of 2

Three-Paged Figure

Supplemental Figure 4. Additional Stool Metabolomics Measurements

(A) Shannon index alpha diversity Pre-NASH and at the time of NASH onset. (B) The number of overlapping features that are significantly increased or decreased at ZT13 (as identified in Figure 7b & 7c) Pre-NASH and at the time of NASH onset. (C) Pre-NASH, the molecular class of features identified as significantly increased at ZT13. (D) Pre-NASH, the molecular class of features identified as significantly decreased at ZT13. (E) At NASH, the molecular class of features identified as significantly increased at ZT13. (F) At NASH, the molecular class of features identified as significantly decreased at ZT13.

Significance thresholds set at +/-1 log2(FoldChange) and p-value of 0.05 (t-test, FDR correction)

S4a.

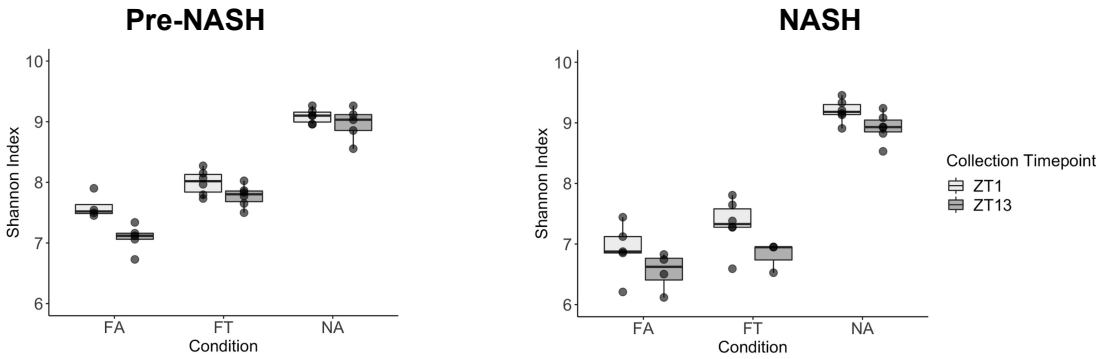

S4b.

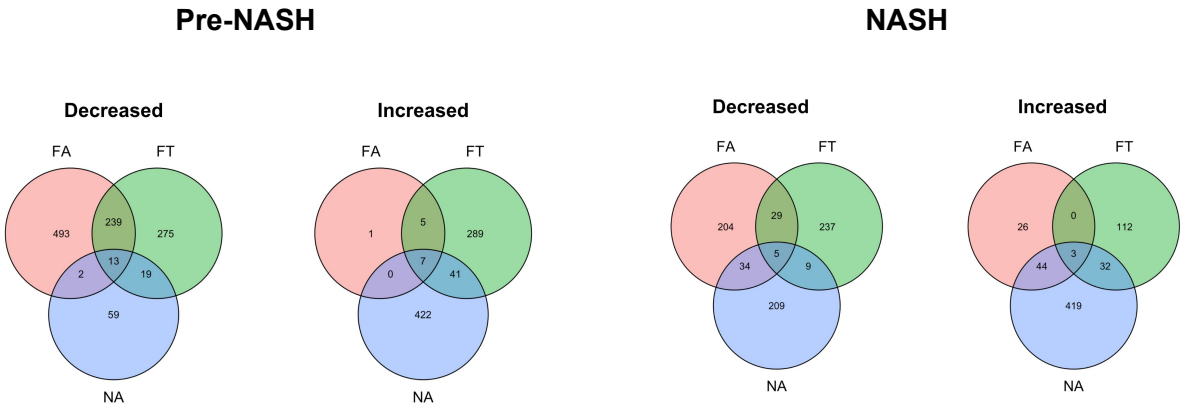

S4c.

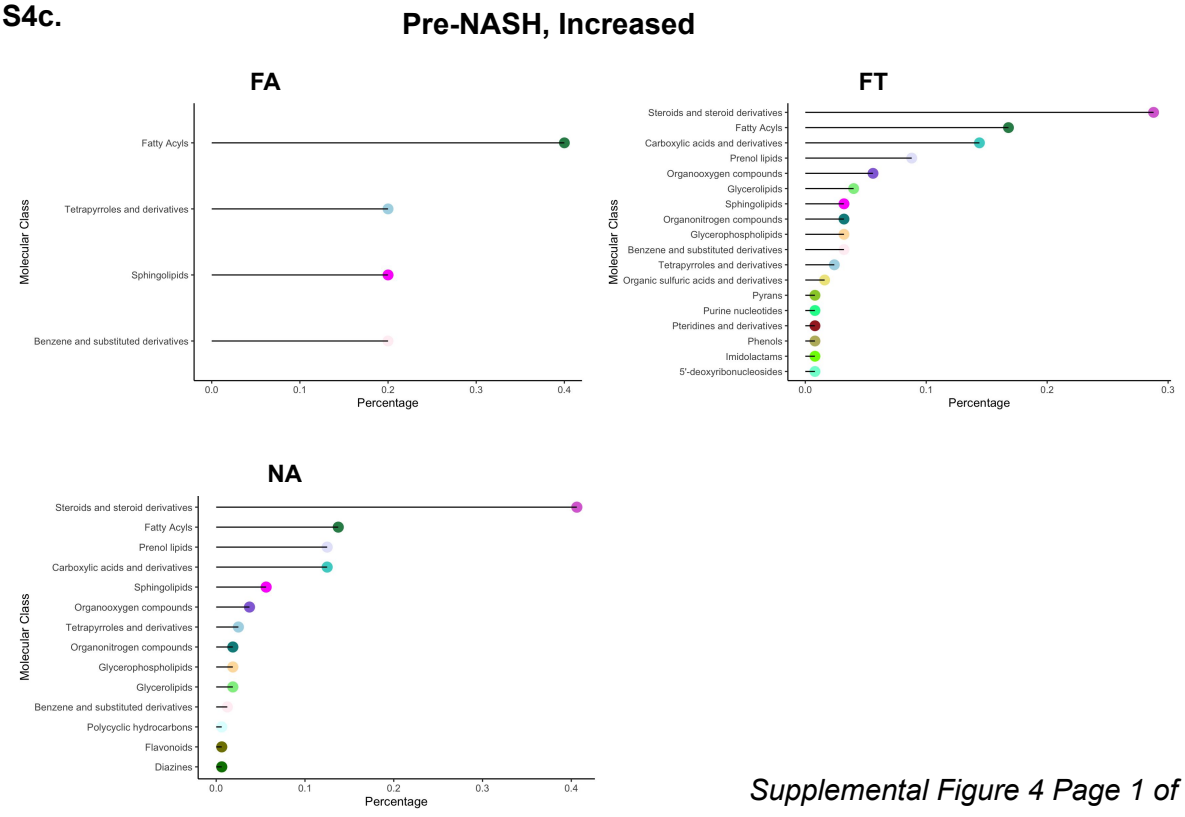

Supplemental Figure 4 Page 1 of 3

S4d.

Pre-NASH, Decreased

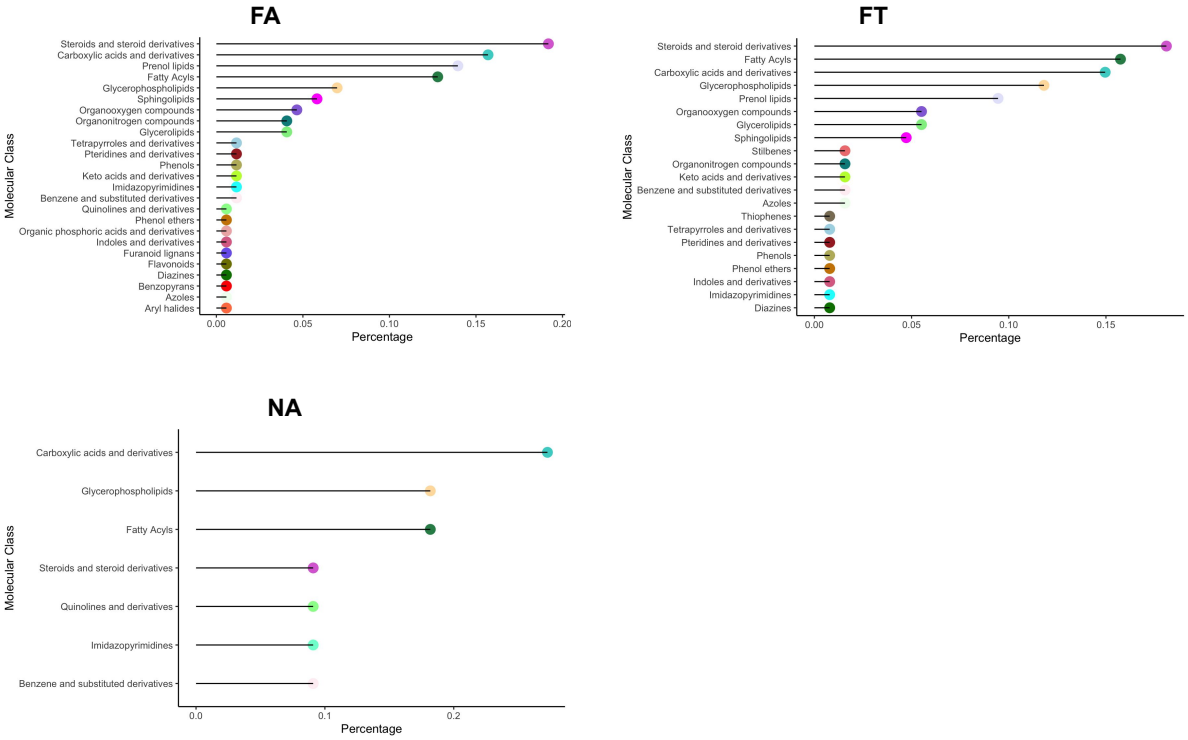

S4e.

NASH, Increased

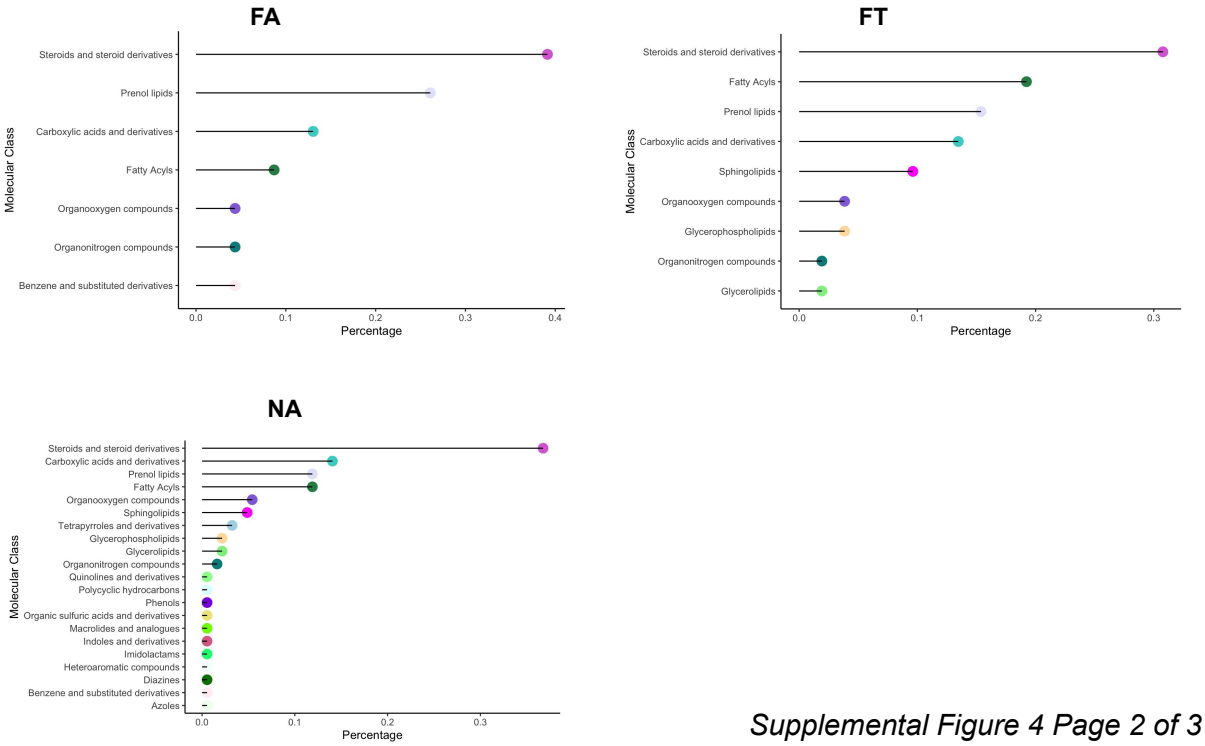

S4f.

NASH, Decreased

FA

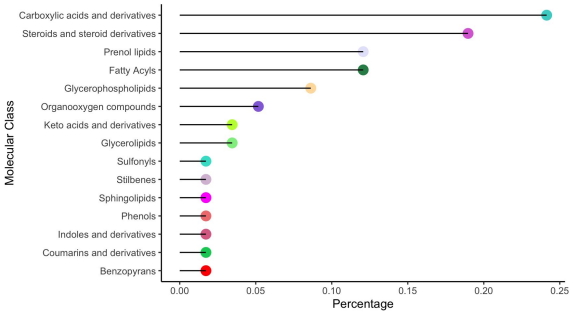

FT

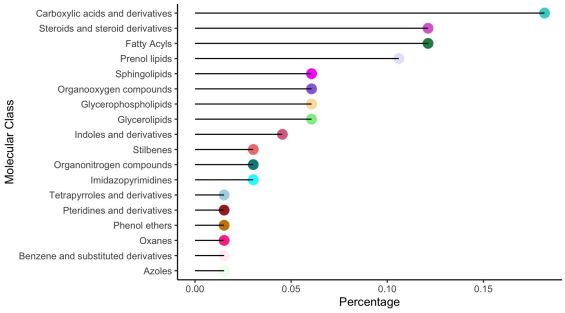

NA

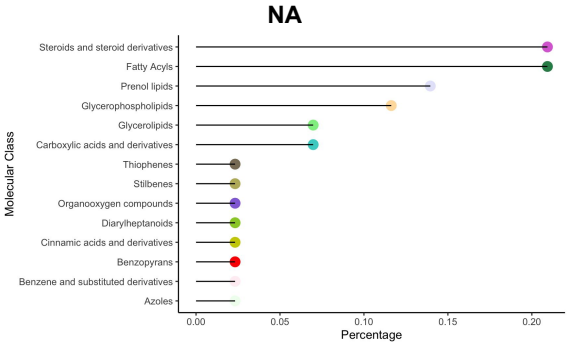

Supplemental Figure 4 Page 3 of 3

Chapter 2 is currently being prepared for submission for publication of the material: “Fogelson, Kelly; Aron, Allegra; Muti, Valentina; Salido Benítez, Rodolfo Antonio; Richter, Roland; Hu, Jingjing; Hosseini, Mojgan; Dorrestein, Pieter; Knight, Rob; Zarrinpar, Amir. Title and Journal Undetermined. (Paper currently in preparation).” The dissertation author is the primary investigator and author of this paper.

Chapter III

The Effect of NASH on Diurnal Transcriptional Patterns
in the Ileum and Liver

3.1. Diurnal Transcriptional Patterns are Maintained in the Ileum During STAM/HFD-Induced NASH

Gut microbially-modified metabolites can impact the host through the modulation of gene expression patterns in the gastrointestinal tract, as well as in peripheral organs such as the liver. Gut microbially-modified metabolites can reach the liver to affect gene expression through the hepatic portal vein, and to a lesser extent, through passive diffusion into systemic circulation. Thus, since our result demonstrated that mice with STAM/HFD-induced NASH (FA and FT conditions) have disruptions to diurnal fluctuations in the gut microbial metabolome, we next investigated the impact that these disruptions may have on transcriptional rhythms in the gastrointestinal tract and liver at the time of NASH onset. To accomplish this, we sacrificed groups of mice at each of two timepoints near NASH onset (12 weeks) to investigate diurnal shifts in transcriptional patterns in the liver and ileum between ZT1 and ZT13 (**Chapter 1, Figure 2)**.

First, we investigated global transcriptional patterns in the ileum with principal component analysis (PCA) (**Fig 8a**). In the ileum, global transcriptional patterns are driven by diet type (FA and FT = HFD, NA= NCD) and the time of sacrifice (ZT1 or ZT13), with FA and FT conditions having a high degree of overlap in transcriptional patterns (**Fig 8a**). PC1 demonstrates that the greatest differences in gene expression are driven by the time of sacrifice (**Fig 8a**). Within each condition, there is no overlap between samples that were harvested at ZT1 vs ZT13. PC2 separates ileum samples based on condition (**Fig 8a**). Although there is a high degree of overlap between FA and FT conditions, PC3 resolves some of this overlap, demonstrating that FA and FT have between group differences in global transcriptional patterns and clear separation based on the time of sacrifice. Overall, results from PCA reveal that global transcriptional patterns in the ileum are driven most strongly by the time of sacrifice (ZT1 or ZT13) and condition (i.e., diet + feeding schedule).

Next, we investigated diurnal shifts in transcriptional patterns in the ileum between ZT1 and ZT13 (**Fig 8b**). To accomplish this, we completed differential gene expression analysis for ileum samples collected at ZT1 or ZT13 for each condition. In the ileum, FT mice have the greatest number of genes with significant differential gene expression between ZT1 and ZT13 (**Fig 8b**). Approximately 5% of genes in the ileum are significantly differentially expressed between ZT1 and ZT13 in FT mice, compared to 3% or less in the ileum of FA and NA mice (**Fig 8b**). However, it should be noted that NA mice have slightly greater diurnal shifts in transcriptional patterns between ZT1 and ZT13 than FA mice.

Next, we performed gene enrichment analysis on genes significantly differentially expressed between ZT1 and ZT13 for each condition (**Fig 8c**). In the ileum, “rhythmic”, “biological”, and “metabolic process” stand out as enriched top level biological processes affected by time of sample collection across conditions (**Fig 8c**). Broadly, many of the gene ontology biological processes identified through enrichment analysis fit within the modulation of host biological, cellular, immune, and signaling processes. Although this information is useful in providing a broad overview of biological processes affected in the ileum by time across all three conditions, it does not provide the resolution necessary to ascertain mechanistic information about differentially expressed genes and pathways, and how transcriptional patterns may varry between conditions. Thus, we next identified differences in the fluctuation of genes of interest between ZT1 and ZT13.

Genes sets of interest were identified using three primary strategies: 1) differentially expressed genes involved in biological processes of interest, identified via enrichment analysis, 2) genes previously identified to be involved in NASH pathogenesis, and 3) genes involved in pathways that may be affected by metabolite subclasses identified in (**Fig 7d and Fig 7e**). To examine differences in diurnal expression patterns, we compared the Log2FoldChange(ZT13/ZT1) for genes of interest across conditions. Surprisingly, we observed

that mice with STAM/HFD-induced NASH (FA and FT conditions) have a maintenance of rhythmic expression patterns relative to mice that don't develop NASH (NA condition) for genes involved in the regulation of circadian rhythms (**Fig 8d**), bile acid reabsorption and transcriptional regulation (**Fig 8e**), and GLP-1 signaling (**Fig 8f**). Overall, genes involved in these biological processes have the same directionality in Log2FoldChange(ZT13/ZT1) across all three conditions, indicating that changes in differential expression are occurring in the same phase of the day. Although there are some minor differences between conditions, circadian patterns of ileal gene expression are not not disrupted during NASH in the STAM/HFD model.

3.2. Diurnal Transcriptional Patterns are Maintained in the Liver During STAM/HFD-Induced NASH

The liver is a hub for the regulation of master metabolic regulators involved in a variety of host homeostatic processes, including glucose, lipid, and bile acid homeostasis. Importantly, master metabolic regulators in the liver, such as *FXR, Ppar, and Sirt1,* can regulate, and are regulated by, the circadian clock [12]. Gut microbiome rhythms can entrain gene expression patterns in the liver through secondary metabolites and nutrients such as bile acids [56,57,80]. Thus, since our result demonstrated that mice with STAM/HFD-induced NASH (FA and FT conditions) have disruptions to diurnal fluctuations in the gut microbial metabolome, we aimed to determine the effect of these disruptions on diurnal gene expression patterns in the liver at the time of NASH onset. To accomplish these, we investigated differences in hepatic transcriptional patterns between ZT1 and ZT13 across conditions from liver samples collected at the same time as animals sacrificed in **Fig 8/Chapter 3.1**.

In the liver, global transcription patterns are most strongly driven by condition (i.e., diet + feeding schedule) with clear separation between all three conditions along PC1 (**Fig 9a**). Although there is some overlap between FA and FT conditions, PC3 resolves this overlap and demonstrates that there are distinct differences between the global transcriptome of these two

conditions. Within each condition, there is no overlap in liver samples collected at ZT1 vs ZT13 along PC2. Overall, results from PCA reveal that global hepatic transcriptional patterns are distinct for each condition and strongly influenced by the time of sacrifice.

Differential gene expression analysis demonstrates that FT mice have the greatest number of genes with significant differential expression between ZT1 and ZT13 (**Fig 9b**). Approximately 7% of genes in the liver are significantly differentially expressed between ZT1 and ZT13 in FT mice, compared to less than 4% in FA and NA mice (**Fig 9b**). As in the ileum, NA mice have slightly stronger diurnal shifts in hepatic transcriptional patterns between ZT1 and ZT13 than FA mice (NA= 3.9%, FA=3.5%).

Gene enrichment analysis was performed on genes significantly differentially expressed between ZT1 and ZT13 for each condition. Analysis identified “rhythmic”, “metabolic”, and “cellular process” as top level biological processes that are influenced by the time of sample collection across conditions (**Fig 9c**). Next, we identified gene sets of interest for relative expression and pathway analysis using the same approaches to identify genes as described in the previous section (**3.1**).

As in the ileum, we observed that mice with STAM/HFD-induced NASH (FA and FT conditions) have a maintenance of rhythmic expression patterns relative to mice that don’t develop NASH (NA condition) for genes involved in the regulation of circadian rhythms (Fig 9d), bile acid synthesis (Fig 9e). Overall, genes involved in these biological processes have the same directionality in Log2FoldChange(ZT13/ZT1) across conditions that develop NASH (FA and FT) and those that don’t (NA), indicating that changes in differential expression are occurring in the same phase of the day. Although there are some minor differences between conditions, overall circadian patterns of hepatic gene expression are not not disrupted during NASH in the STAM/HFD model.

3.3. Discussion

Our results demonstrate that diurnal fluctuations in ileal and hepatic gene expression patterns are not disrupted in mice with STAM/HFD-induced NASH. Gene enrichment analysis on genes that are significantly differentially expressed between ZT1 and ZT13 reveals that similar biological processes are affected by time across all three conditions. Biological processes involved in rhythmic, metabolic, and cellular processes have differential expression between ZT1 and ZT13 in the liver and ileum in mice that develop NASH (FA and FT), as well as those that do not (NA). This suggests that these processes are not involved in the development of NASH in the STAM/HFD model.

Comparison of the Log2FoldChange(ZT13/ZT1) values for genes of interest across conditions revealed that rhythmic expression patterns for genes involved in the regulation of circadian rhythms, bile acid synthesis, and ileal GLP-1 signaling are maintained during STAM/HFD-induced NASH. This suggests that the disruption of hepatic and ileal transcriptional rhythms is not implicated in STAM/HFD-induced NASH pathogenesis. We hypothesize that the maintenance of rhythmic feeding patterns in mice with STAM/HFD-induced NASH (**Chapter 2.3/Fig 4**) may be the primary entrainment signal of circadian rhythms in the liver and the ileum, trumping disruptions that were observed in gut microbiome and metabolome rhythms (**Chapter 2.4-2.6/Fig 5-7**). Overall, our results demonstrate that TRF is not capable of preventing NASH in the STAM/HFD model via the modulation of circadian rhythms. Given that STAM-injected mice are hypoinsulinemic, our findings suggest that insulin may be required to mediate the protective effects of TRF that have been observed across previous studies.

3.4. Research Methods

3.4.a. Experimental Methods

Animal Model, Weight and Food Intake,Feeding Pattern Manipulation, and Sacrifice: the same animals and methods were used as in **Chapter 2.8.a.**

RNA-Sequencing Sample Extraction: Ileum and liver tissue samples were flash frozen in liquid nitrogen and stored at -80℃ until preparation for RNA extraction. Frozen tissue samples were powderized using a mortar and pestle on dry ice prior to completing RNA extractions. For ileum samples, a total nucleic acid extraction was completed on powderized tissue as described in (**Chapter 2**). For liver samples, RNA extractions were completed using the MagMAX mirVana™ Total RNA Isolation Kit (Thermo Fisher Scientific catalog #A27828) on the MagMAX Express 96 Instrument (protocol number: AM1830DW).

3.4.b. Data and Statistical Analysis

RNA-Sequencing: For ileum samples, quality control and library preparation was performed in the Knight Lab at UC San Diego. Sequencing was performed on the Illumina NovaSeq S4 platform using 150PE reads. For liver samples, quality control and library preparation was performed at the Institute for Genomic Medicine core at UC San Diego. Sequencing was performed on the Illumina NovaSeq S4 platform using 100PE reads. Reads were mapped to the mouse genome (GRCm38.p5) using hisat2 v2.2.1 [81], and genes and transcripts were quantified using stringtie v2.1.7 [82]. Gene-level counts were used in all downstream analyses. Differential expression analysis between ZT1 and ZT13 for each condition was performed using DESeq2 [83], with fold changes determined using the normal method for all transcripts whose counts were greater than 100 in at least three samples (per each tissue type). For volcano plots, statistical significance thresholds were set at Log2Foldchange at least +/- 2 for ileum samples and at least +/-1 for liver samples, and an adjusted p-value of at least 10e-6 (Wald, Benjamini-Hochberg correction). Gene enrichment analysis was performed with Metascape [84], and additional graphing was completed in R Studio.

Three-Paged Figure

Figure 8. Diurnal Transcriptional Patterns in the Ileum are Maintained During STAM/HFD-induced NASH

(A) PCA Analysis across all data (all collection time points included). Differences in ileal transcriptome are driven by time of sacrifice and diet-type. (B) Volcano plots of Log2Foldchange(ZT13/ZT1) per each condition. Genes significantly increased (up) or decreased (down) at ZT13 are shown in red. Percentage of transcripts in each category shown on the right. Significance thresholds set at Log2Foldchange at least +/- 2 and adjusted p-value of at least 10e-6 (Wald, Benjamini-Hochberg correction). (C) Top-level gene ontology biological process for significantly increased and decreased genes per each condition, determined by Metascape. Log2FoldChange(ZT13/ZT1) for (D) circadian rhythm, (E) bile acid, and (F) GLP-1 signaling genes.

8a. Ileum Transcriptomics : All Data

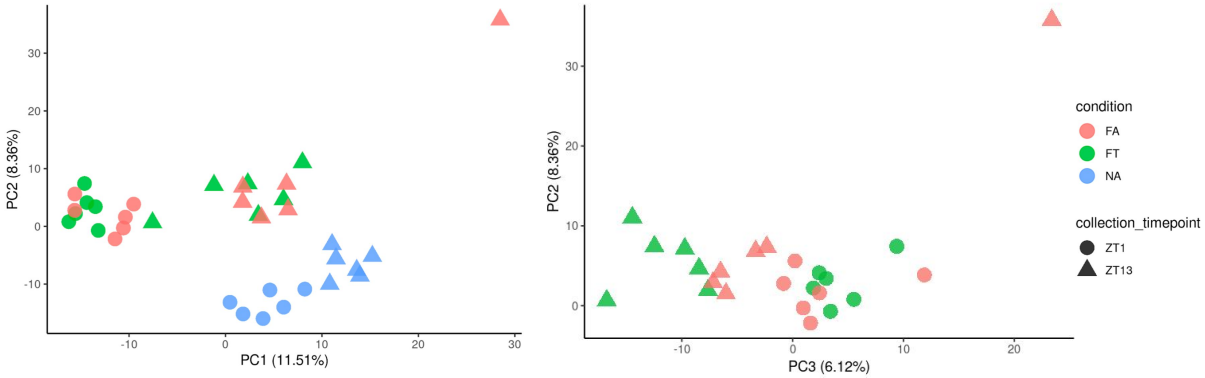

8b. Log2FoldChange(ZT13/ZT1)

8c. Top-Level Gene Ontology Biological Process

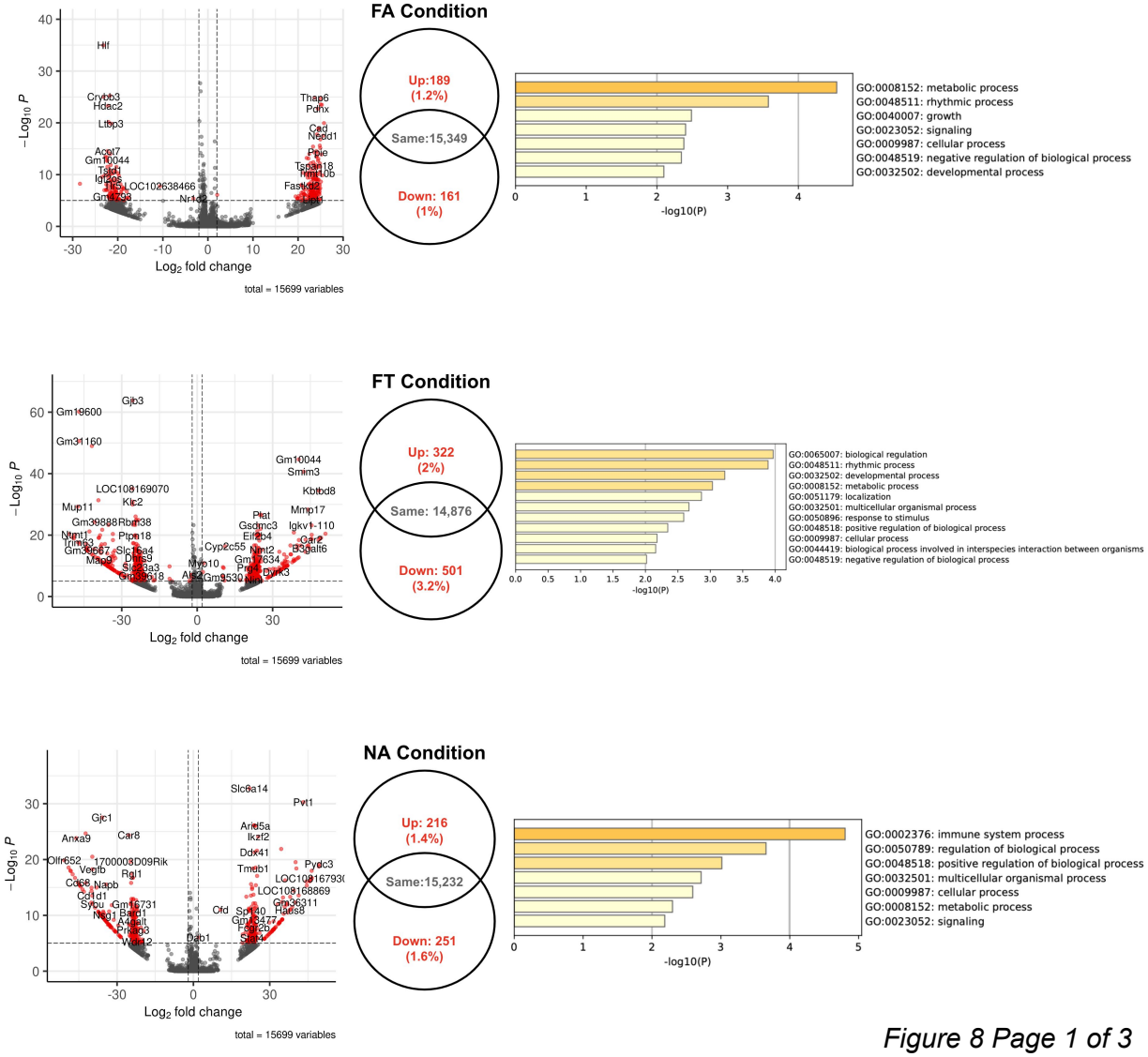

Figure 8 Page 1 of 3

8d.

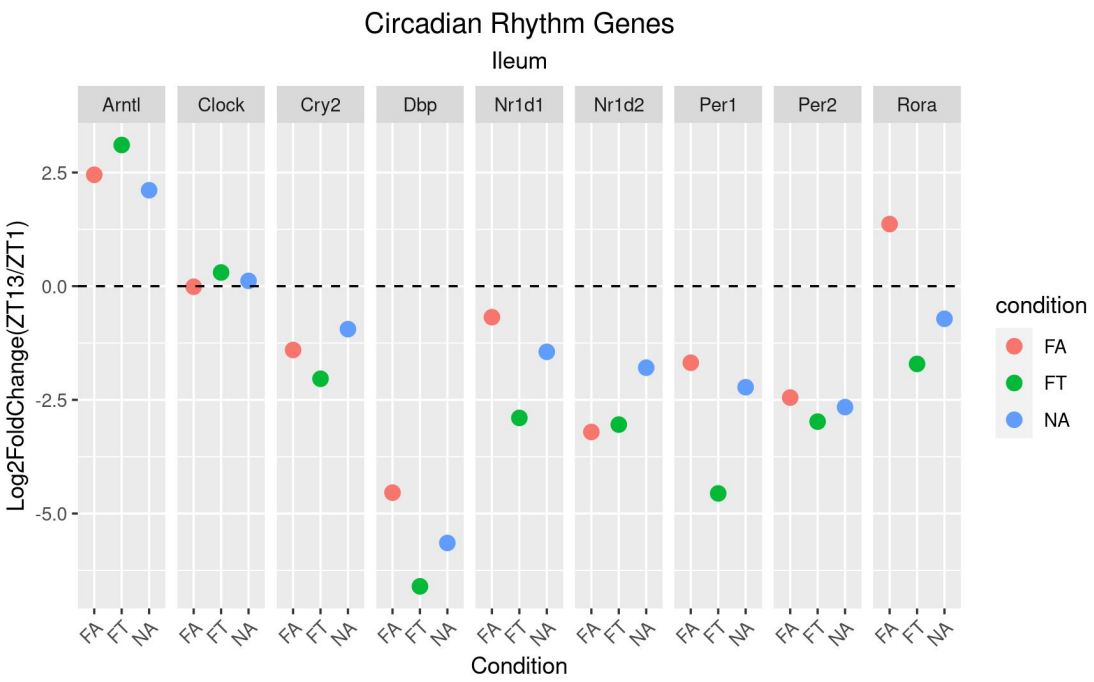

8e.

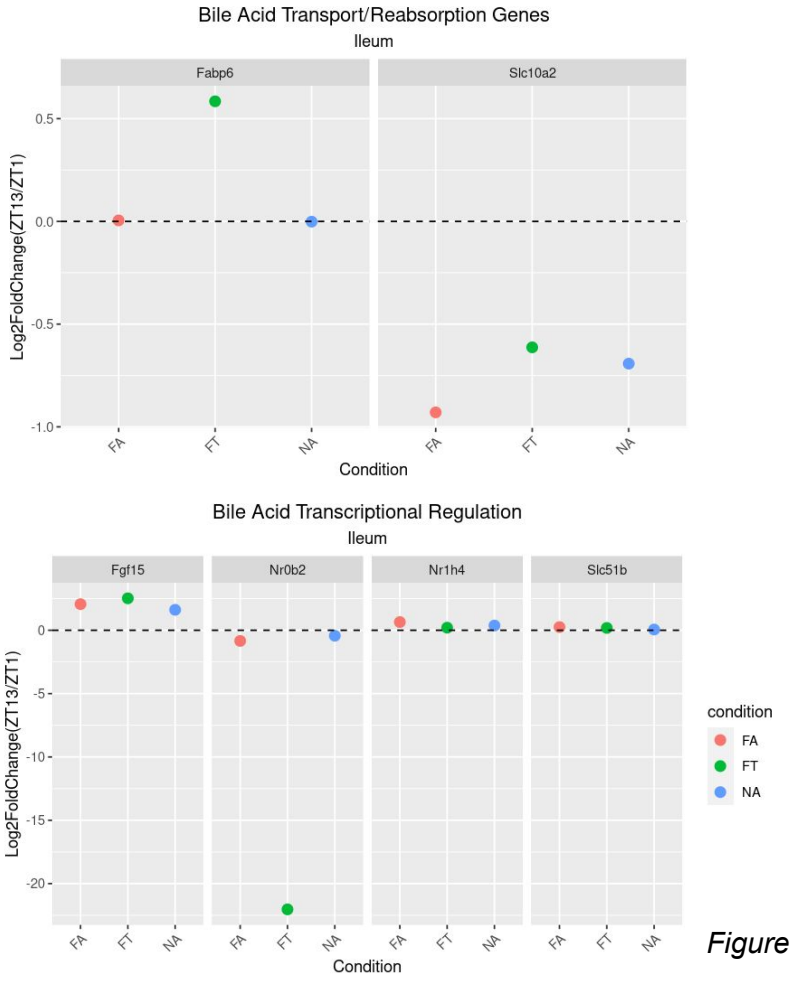

Figure 8 Page 2 of 3

8f.

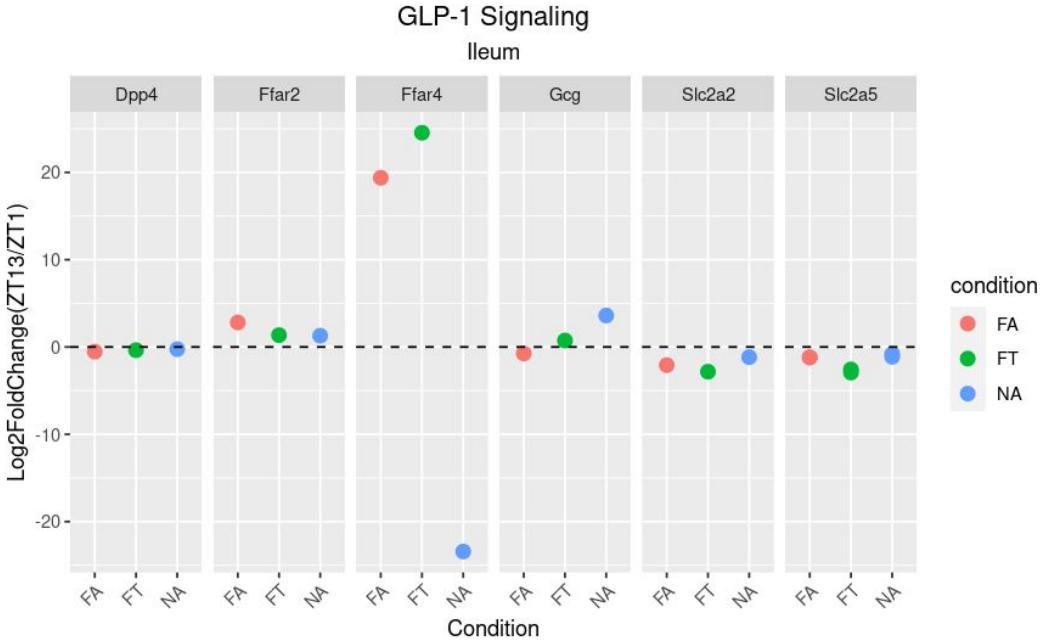

Figure 8 Page 3 of 3

Two-Paged Figure

Figure 9. Diurnal Transcriptional Patterns in the Liver are Maintained During STAM/HFD-induced NASH

(A) PCA Analysis across all data (all collection time points included). Differences in liver transcriptome are driven by condition and time of sacrifice. (B) Volcano plots of Log2Foldchange(ZT13/ZT1) per each condition. Genes significantly increased (up) or decreased (down) at ZT13 are shown in red. Percentage of transcripts in each category shown on the right. Significance thresholds set at Log2Foldchange at least +/- 1 and adjusted p-value of at least 10e-6 (Wald, Benjamini-Hochberg correction). (C) Top-level gene ontology biological process for significantly increased and decreased genes per each condition, determined by Metascape. (D) Log2FoldChange(ZT13/ZT1) for circadian rhythm genes of interest (E) Log2FoldChange(ZT13/ZT1) for bile acid and bile salt synthesis genes.

9a. Liver Transcriptomics : All Data

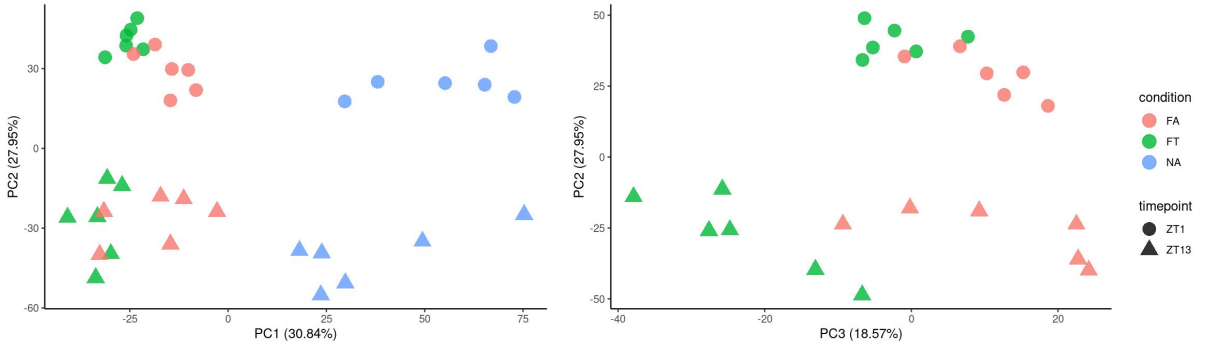

9b. Log2FoldChange(ZT13/ZT1)

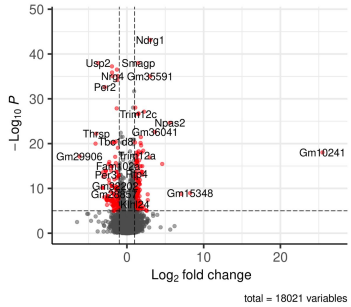

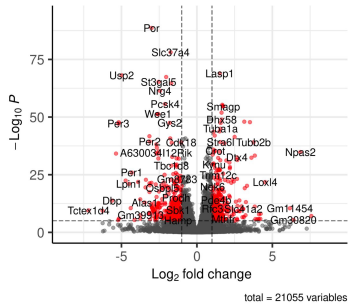

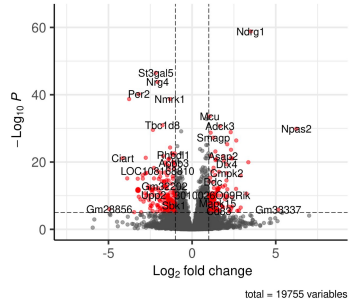

9c. Top-Level Gene Ontology Biological Process

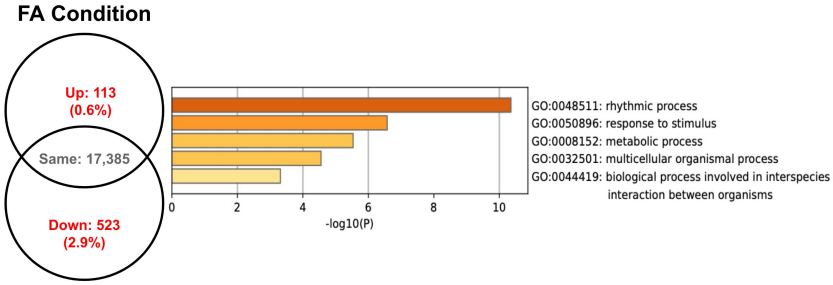

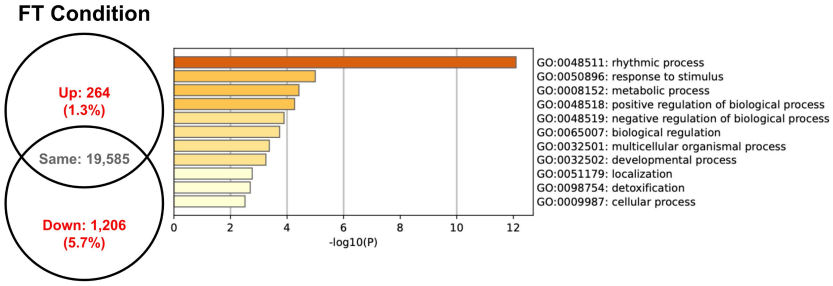

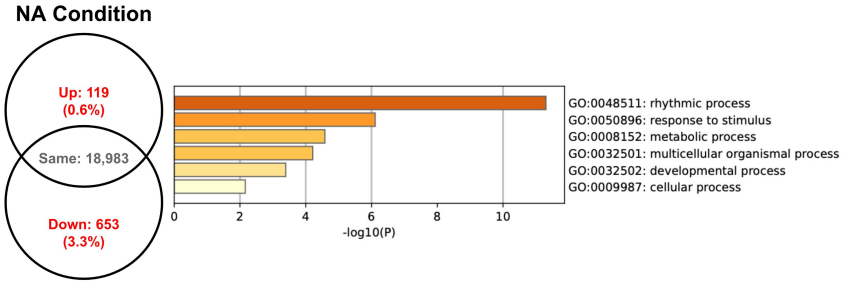

Figure 9 Page 1 of 2

9d.

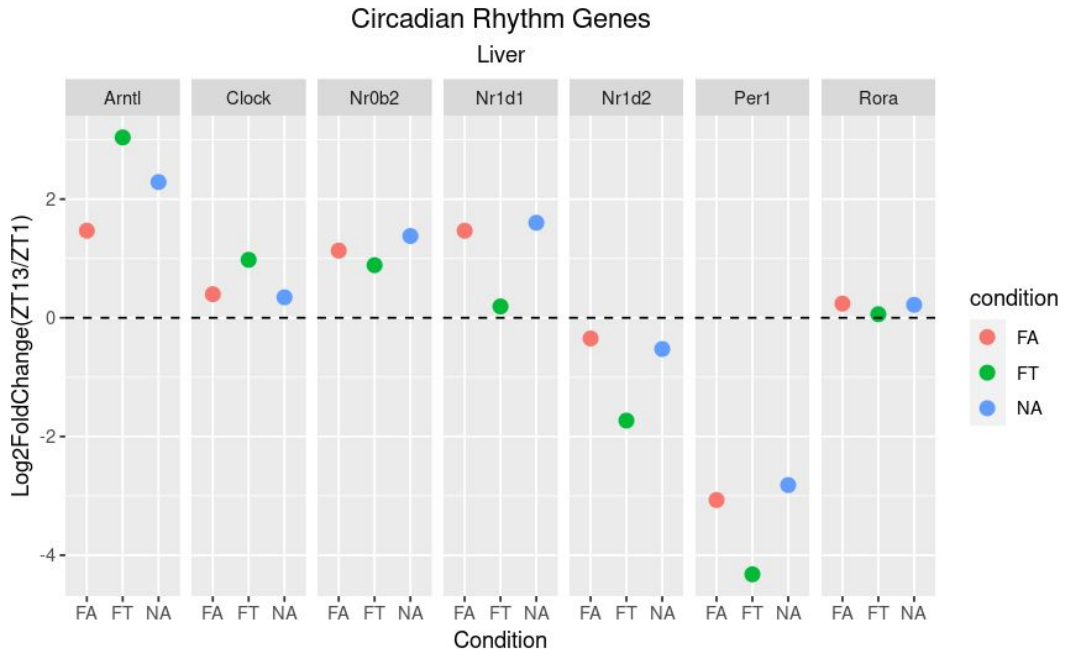

9e.

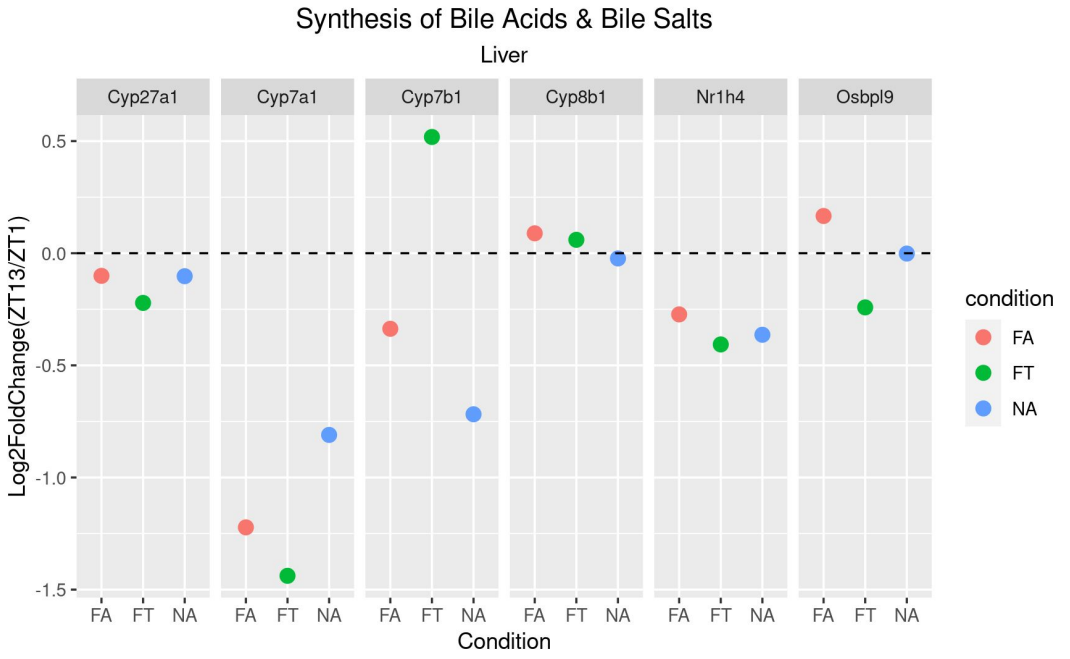

Figure 9 Page 2 of 2

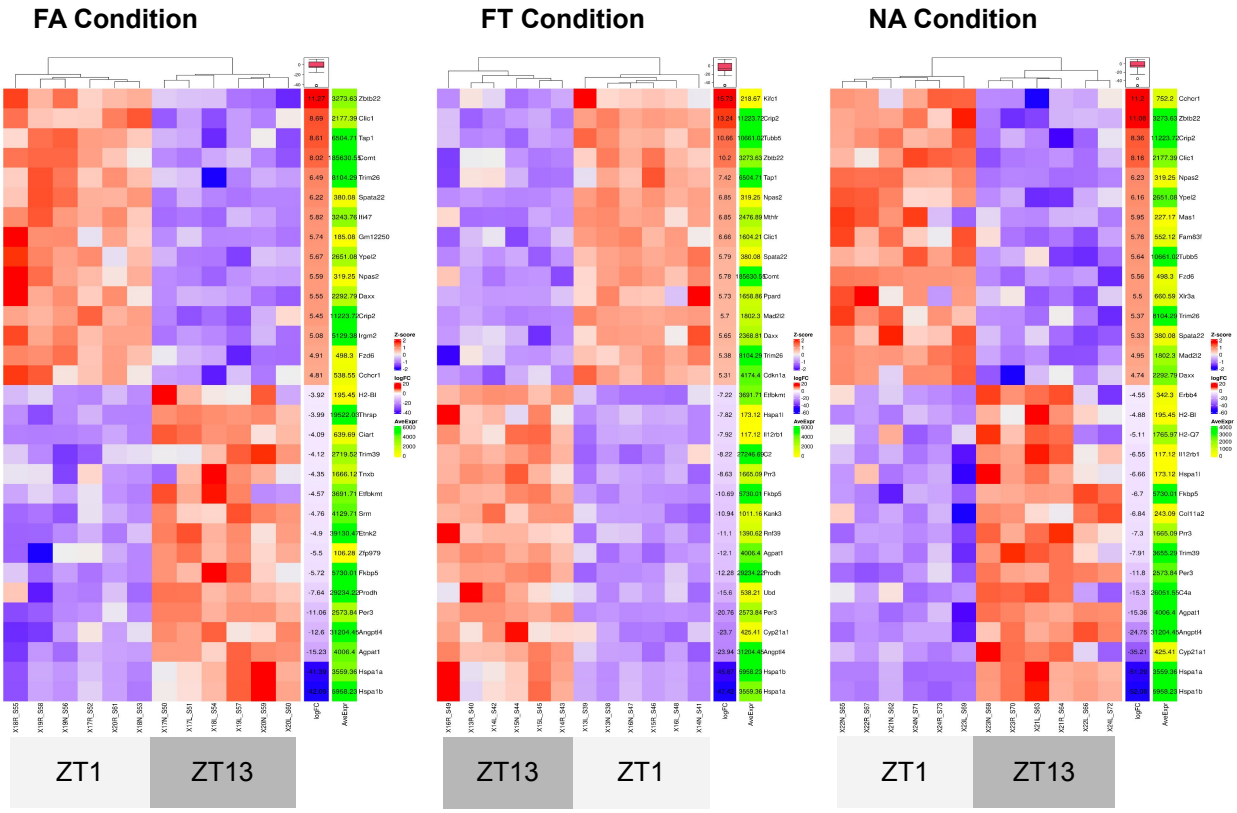

Supplemental Figure 5. Liver Transcriptomics Heat Map
Heat maps per each condition and ZT. Genes were filtered for based on normalized expression (BaseMean) and high differential expression between ZT1 and ZT13. The top and bottom 15 genes are shown with Base Mean >100 and Log2Foldchange of +/-2. Columns to the right of each heatmap display log2Foldchange and BaseMean(AveExpr) for the indicated gene.

Chapter 3 is currently being prepared for submission for publication of the material: “Fogelson, Kelly; Aron, Allegra; Muti, Valentina; Salido Benítez, Rodolfo Antonio; Richter, Roland; Hu, Jingjing; Hosseini, Mojgan; Dorrestein, Pieter; Knight, Rob; Zarrinpar, Amir. Title and Journal Undetermined. (Paper currently in preparation).” The dissertation author is the primary investigator and author of this paper.

Summary

The overall objective of this study was to elucidate the role of circadian dyssynchrony in the pathophysiology and progression of NAFLD-associated NASH. We hypothesized that NASH results from altered gut microbiome dynamics and disrupted hepatic and intestinal circadian rhythms, which could be manipulated with TRF to ameliorate disease. Utilization of the STAM/HFD murine model of NASH, in which mice are hypoinsulinemic, allowed us to specifically investigate whether TRF could prevent NASH via the modulation of circadian rhythms, without the confounding factor of TRF affecting insulin signaling. Findings from this study reveal that TRF is capable of preventing disruptions to diurnal fluctuations in gut microbiome composition in STAM/HFD mice with adlib access to food. However, TRF is not capable of preventing NASH in the STAM/HFD model. Surprisingly, STAM/HFD mice with adlib access to food have a maintenance of rhythmic feeding patterns, as well as an overall maintenance of ileal and hepatic gene expression patterns. Altogether, this suggests that the maintenance of rhythmic feeding patterns in mice with STAM/HFD-induced NASH may be the primary entrainment signal of circadian rhythms in the liver and the ileum, trumping disruptions that are observed in gut microbiome and/or metabolome rhythms. Results from this study suggest that STAM/HFD-induced NASH does not result from circadian rhythm disruption, and that insulin may be a crucial element to mediating the protective effects of TRF.

References

1. Younossi ZM. Non-alcoholic fatty liver disease - A global public health perspective. J Hepatol. 2019 Mar;70(3):531–44.
2. Definition & Facts of NAFLD & NASH | NIDDK [Internet]. [cited 2020 Jun 13]. Available from: https://www.niddk.nih.gov/health-information/liver-disease/nafld-nash/definition-facts
3. NASH Definition & Prevalence — American Liver Foundation [Internet]. [cited 2021 Dec 9]. Available from: https://liverfoundation.org/for-patients/about-the-liver/diseases-of-the-liver/nonalcoholic-steatohepatitis-information-center/nash-definition-prevalence/
4. Buzzetti E, Pinzani M, Tsochatzis EA. The multiple-hit pathogenesis of non-alcoholic fatty liver disease (NAFLD). Metab Clin Exp. 2016 Aug;65(8):1038–48.
5. Zarrinpar A, Chaix A, Yooseph S, Panda S. Diet and feeding pattern affect the diurnal dynamics of the gut microbiome. Cell Metab. 2014 Dec 2;20(6):1006–17.
6. Hatori M, Vollmers C, Zarrinpar A, DiTacchio L, Bushong EA, Gill S, Leblanc M, Chaix A, Joens M, Fitzpatrick JAJ, Ellisman MH, Panda S. Time-restricted feeding without reducing caloric intake prevents metabolic diseases in mice fed a high-fat diet. Cell Metab. 2012 Jun 6;15(6):848–60.
7. Fujii M, Shibazaki Y, Wakamatsu K, Honda Y, Kawauchi Y, Suzuki K, Arumugam S, Watanabe K, Ichida T, Asakura H, Yoneyama H. A murine model for non-alcoholic steatohepatitis showing evidence of association between diabetes and hepatocellular carcinoma. Med Mol Morphol. 2013 Sep;46(3):141–52.
8. Ruissen MM, Mak AL, Beuers U, Tushuizen ME, Holleboom AG. Non-alcoholic fatty liver disease: a multidisciplinary approach towards a cardiometabolic liver disease. Eur J Endocrinol. 2020 Sep;183(3):R57–73.
9. Vilar-Gomez E, Martinez-Perez Y, Calzadilla-Bertot L, Torres-Gonzalez A, Gra-Oramas B, Gonzalez-Fabian L, Friedman SL, Diago M, Romero-Gomez M. Weight loss through lifestyle modification significantly reduces features of nonalcoholic steatohepatitis. Gastroenterology. 2015 Aug;149(2):367-78.e5; quiz e14.
10. Wilkinson MJ, Manoogian ENC, Zadourian A, Lo H, Fakhouri S, Shoghi A, Wang X, Fleischer JG, Navlakha S, Panda S, Taub PR. Ten-Hour Time-Restricted Eating Reduces Weight, Blood Pressure, and Atherogenic Lipids in Patients with Metabolic Syndrome. Cell Metab. 2020 Jan 7;31(1):92-104.e5.
11. Gnocchi D, Custodero C, Sabbà C, Mazzocca A. Circadian rhythms: a possible new player in non-alcoholic fatty liver disease pathophysiology. J Mol Med. 2019 Jun;97(6):741–59.
12. Saran AR, Dave S, Zarrinpar A. Circadian rhythms in the pathogenesis and treatment of fatty liver disease. Gastroenterology. 2020 May;158(7):1948-1966.e1.
13. Choi H, Rao MC, Chang EB. Gut microbiota as a transducer of dietary cues to regulate host circadian rhythms and metabolism. Nat Rev Gastroenterol Hepatol. 2021

Oct;18(10):679–89.

14. Liu S, Qin P, Wang J. High-Fat Diet Alters the Intestinal Microbiota in Streptozotocin-Induced Type 2 Diabetic Mice. Microorganisms. 2019 Jun 16;7(6).

15. Lang S, Schnabl B. Microbiota and Fatty Liver Disease-the Known, the Unknown, and the Future. Cell Host Microbe. 2020 Aug 12;28(2):233–44.

16. Chaix A, Zarrinpar A, Miu P, Panda S. Time-restricted feeding is a preventative and therapeutic intervention against diverse nutritional challenges. Cell Metab. 2014 Dec 2;20(6):991–1005.

17. Tripathi A, Debelius J, Brenner DA, Karin M, Loomba R, Schnabl B, Knight R. The gut-liver axis and the intersection with the microbiome. Nat Rev Gastroenterol Hepatol. 2018 Jul;15(7):397–411.

18. Spengler EK, Loomba R. Recommendations for diagnosis, referral for liver biopsy, and treatment of nonalcoholic fatty liver disease and nonalcoholic steatohepatitis. Mayo Clin Proc. 2015 Sep;90(9):1233–46.

19. Graham ML, Janecek JL, Kittredge JA, Hering BJ, Schuurman H-J. The streptozotocin-induced diabetic nude mouse model: differences between animals from different sources. Comp Med. 2011 Aug;61(4):356–60.

20. Takakura K, Oikawa T, Tomita Y, Mizuno Y, Nakano M, Saeki C, Torisu Y, Saruta M. Mouse models for investigating the underlying mechanisms of nonalcoholic steatohepatitis-derived hepatocellular carcinoma. World J Gastroenterol. 2018 May 14;24(18):1989–94.

21. Van Herck MA, Vonghia L, Francque SM. Animal Models of Nonalcoholic Fatty Liver Disease-A Starter's Guide. Nutrients. 2017 Sep 27;9(10).

22. López-Otín C, Kroemer G. Hallmarks of Health. Cell. 2021 Jan 7;184(1):33–63.

23. Chaix A, Zarrinpar A, Panda S. The circadian coordination of cell biology. J Cell Biol. 2016 Oct 10;215(1):15–25.

24. Sender R, Fuchs S, Milo R. Are we really vastly outnumbered? revisiting the ratio of bacterial to host cells in humans. Cell. 2016 Jan 28;164(3):337–40.

25. Gilbert JA, Blaser MJ, Caporaso JG, Jansson JK, Lynch SV, Knight R. Current understanding of the human microbiome. Nat Med. 2018 Apr 10;24(4):392–400.

26. NIH Human Microbiome Project defines normal bacterial makeup of the body | National Institutes of Health (NIH) [Internet]. [cited 2022 Sep 12]. Available from: https://www.nih.gov/news-events/news-releases/nih-human-microbiome-project-defines-normal-bacterial-makeup-body

27. Leone V, Gibbons SM, Martinez K, Hutchison AL, Huang EY, Cham CM, Pierre JF, Heneghan AF, Nadimpalli A, Hubert N, Zale E, Wang Y, Huang Y, Theriault B, Dinner AR, Musch MW, Kudsk KA, Prendergast BJ, Gilbert JA, Chang EB. Effects of diurnal variation of gut microbes and high-fat feeding on host circadian clock function and metabolism. Cell Host Microbe. 2015 May 13;17(5):681–9.

28. Thaiss CA, Zeevi D, Levy M, Zilberman-Schapira G, Suez J, Tengeler AC, Abramson L, Katz MN, Korem T, Zmora N, Kuperman Y, Biton I, Gilad S, Harmelin A, Shapiro H, Halpern Z, Segal E, Elinav E. Transkingdom control of microbiota diurnal oscillations promotes metabolic homeostasis. Cell. 2014 Oct 23;159(3):514–29.

29. Thaiss CA, Levy M, Korem T, Dohnalová L, Shapiro H, Jaitin DA, David E, Winter DR, Gury-BenAri M, Tatirovsky E, Tuganbaev T, Federici S, Zmora N, Zeevi D, Dori-Bachash M, Pevsner-Fischer M, Kartvelishvily E, Brandis A, Harmelin A, Shibolet O, Elinav E. Microbiota diurnal rhythmicity programs host transcriptome oscillations. Cell. 2016 Dec 1;167(6):1495-1510.e12.

30. Liang X, Bushman FD, FitzGerald GA. Rhythmicity of the intestinal microbiota is regulated by gender and the host circadian clock. Proc Natl Acad Sci USA. 2015 Aug 18;112(33):10479–84.

31. Zarrinpar A, Chaix A, Panda S. Daily eating patterns and their impact on health and disease. Trends Endocrinol Metab. 2016 Feb;27(2):69–83.

32. Weger BD, Gobet C, Yeung J, Martin E, Jimenez S, Betrisey B, Foata F, Berger B, Balvay A, Foussier A, Charpagne A, Boizet-Bonhoure B, Chou CJ, Naef F, Gachon F. The Mouse Microbiome Is Required for Sex-Specific Diurnal Rhythms of Gene Expression and Metabolism. Cell Metab. 2019 Feb 5;29(2):362-382.e8.

33. Greenwell BJ, Trott AJ, Beytebiere JR, Pao S, Bosley A, Beach E, Finegan P, Hernandez C, Menet JS. Rhythmic Food Intake Drives Rhythmic Gene Expression More Potently than the Hepatic Circadian Clock in Mice. Cell Rep. 2019 Apr 16;27(3):649-657.e5.

34. Chiang JYL. Bile acid metabolism and signaling. Compr Physiol. 2013 Jul;3(3):1191–212.

35. de Aguiar Vallim TQ, Tarling EJ, Edwards PA. Pleiotropic roles of bile acids in metabolism. Cell Metab. 2013 May 7;17(5):657–69.

36. Wahlström A, Sayin SI, Marschall H-U, Bäckhed F. Intestinal Crosstalk between Bile Acids and Microbiota and Its Impact on Host Metabolism. Cell Metab. 2016 Jul 12;24(1):41–50.

37. Quinn RA, Melnik AV, Vrbanac A, Fu T, Patras KA, Christy MP, Bodai Z, Belda-Ferre P, Tripathi A, Chung LK, Downes M, Welch RD, Quinn M, Humphrey G, Panitchpakdi M, Weldon KC, Aksenov A, da Silva R, Avila-Pacheco J, Clish C, Dorrestein PC. Global chemical effects of the microbiome include new bile-acid conjugations. Nature. 2020 Mar;579(7797):123–9.

38. Dethloff F, Vargas F, Elijah E, Quinn R, Park DI, Herzog DP, Müller MB, Gentry EC, Knight R, Gonzalez A, Dorrestein PC, Turck CW. Paroxetine administration affects microbiota and bile acid levels in mice. Front Psychiatry. 2020 Jun 4;11:518.

39. Petras D, Caraballo-Rodríguez AM, Jarmusch AK, Molina-Santiago C, Gauglitz JM, Gentry EC, Belda-Ferre P, Romero D, Tsunoda SM, Dorrestein PC, Wang M. Chemical Proportionality within Molecular Networks. Anal Chem. 2021 Sep 28;93(38):12833–9.

40. Dorrestein P, Gentry E, Collins S, Panitchpakdi M, Belda-Ferre P, Stewart A, Wang M, Jarmusch A, Avila-Pacheco J, Plichta D, Aron A, Vlamakis H, Ananthakrishnan A, Clish C, Xavier R, Baker E, Patterson A, Knight R, Siegel D. A Synthesis-Based Reverse

Metabolomics Approach for the Discovery of Chemical Structures from Humans and Animals. Res Sq. 2021 Aug 30;

41. Wang M, Jarmusch AK, Vargas F, Aksenov AA, Gauglitz JM, Weldon K, Petras D, da Silva R, Quinn R, Melnik AV, van der Hooft JJJ, Caraballo-Rodríguez AM, Nothias LF, Aceves CM, Panitchpakdi M, Brown E, Di Ottavio F, Sikora N, Elijah EO, Labarta-Bajo L, Dorrestein PC. Mass spectrometry searches using MASST. Nat Biotechnol. 2020 Jan;38(1):23–6.

42. Hoffmann MA, Nothias L-F, Ludwig M, Fleischauer M, Gentry EC, Witting M, Dorrestein PC, Dührkop K, Böcker S. High-confidence structural annotation of metabolites absent from spectral libraries. Nat Biotechnol. 2022 Mar;40(3):411–21.

43. Ridlon JM, Harris SC, Bhowmik S, Kang D-J, Hylemon PB. Consequences of bile salt biotransformations by intestinal bacteria. Gut Microbes. 2016;7(1):22–39.

44. Joyce SA, Shanahan F, Hill C, Gahan CGM. Bacterial bile salt hydrolase in host metabolism: Potential for influencing gastrointestinal microbe-host crosstalk. Gut Microbes. 2014;5(5):669–74.

45. Joyce SA, Gahan CGM. Bile Acid Modifications at the Microbe-Host Interface: Potential for Nutraceutical and Pharmaceutical Interventions in Host Health. Annu Rev Food Sci Technol. 2016 Jan 11;7:313–33.

46. Watanabe M, Houten SM, Mataki C, Christoffolete MA, Kim BW, Sato H, Messaddeq N, Harney JW, Ezaki O, Kodama T, Schoonjans K, Bianco AC, Auwerx J. Bile acids induce energy expenditure by promoting intracellular thyroid hormone activation. Nature. 2006 Jan 26;439(7075):484–9.

47. Selwyn F, Klaassen CD. Characterization of Bile Acid homeostasis in Germ‐free Mice. The FASEB Journal. 2012 Apr 1;

48. Gustafsson BE, Midtvedt T, Norman A. Metabolism of cholic acid in germfree animals after the establishment in the intestinal tract of deconjugating and 7 alpha-dehydroxylating bacteria. Acta Pathol Microbiol Scand. 1968;72(3):433–43.

49. Midtvedt T, Norman A. Bile acid transformations by microbial strains belonging to genera found in intestinal contents. Acta Pathol Microbiol Scand. 1967;71(4):629–38.

50. Gustafsson BE, Midtvedt T, Norman A. Isolated fecal microorganisms capable of 7-alpha-dehydroxylating bile acids. J Exp Med. 1966 Feb 1;123(2):413–32.

51. Zarrinpar A, Chaix A, Xu ZZ, Chang MW, Marotz CA, Saghatelian A, Knight R, Panda S. Antibiotic-induced microbiome depletion alters metabolic homeostasis by affecting gut signaling and colonic metabolism. Nat Commun. 2018 Jul 20;9(1):2872.

52. Matsubara T, Li F, Gonzalez FJ. FXR signaling in the enterohepatic system. Mol Cell Endocrinol. 2013 Apr 10;368(1–2):17–29.

53. Pols TWH, Noriega LG, Nomura M, Auwerx J, Schoonjans K. The bile acid membrane receptor TGR5 as an emerging target in metabolism and inflammation. J Hepatol. 2011 Jun;54(6):1263–72.

54. Fiorucci S, Carino A, Baldoni M, Santucci L, Costanzi E, Graziosi L, Distrutti E, Biagioli M. Bile acid signaling in inflammatory bowel diseases. Dig Dis Sci. 2021 Mar;66(3):674–93.

55. Dantas Machado AC, Brown SD, Lingaraju A, Sivaganesh V, Martino C, Chaix A, Zhao P, Pinto AFM, Chang MW, Richter RA, Saghatelian A, Saltiel AR, Knight R, Panda S, Zarrinpar A. Diet and feeding pattern modulate diurnal dynamics of the ileal microbiome and transcriptome. Cell Rep. 2022 Jul 5;40(1):111008.

56. Frazier K, Chang EB. Intersection of the gut microbiome and circadian rhythms in metabolism. Trends Endocrinol Metab. 2020 Jan;31(1):25–36.

57. Bishehsari F, Voigt RM, Keshavarzian A. Circadian rhythms and the gut microbiota: from the metabolic syndrome to cancer. Nat Rev Endocrinol. 2020 Dec;16(12):731–9.

58. Mouzaki M, Wang AY, Bandsma R, Comelli EM, Arendt BM, Zhang L, Fung S, Fischer SE, McGilvray IG, Allard JP. Bile Acids and Dysbiosis in Non-Alcoholic Fatty Liver Disease. PLoS ONE. 2016 May 20;11(5):e0151829.

59. Caussy C, Hsu C, Singh S, Bassirian S, Kolar J, Faulkner C, Sinha N, Bettencourt R, Gara N, Valasek MA, Schnabl B, Richards L, Brenner DA, Hofmann AF, Loomba R. Serum bile acid patterns are associated with the presence of NAFLD in twins, and dose-dependent changes with increase in fibrosis stage in patients with biopsy-proven NAFLD. Aliment Pharmacol Ther. 2019 Jan;49(2):183–93.

60. Armstrong LE, Guo GL. Role of FXR in Liver Inflammation during Nonalcoholic Steatohepatitis. Curr Pharmacol Rep. 2017 Apr;3(2):92–100.

61. Zhu Y, Liu H, Zhang M, Guo GL. Fatty liver diseases, bile acids, and FXR. Acta Pharm Sin B. 2016 Sep;6(5):409–12.

62. Pathak P, Liu H, Boehme S, Xie C, Krausz KW, Gonzalez F, Chiang JYL. Farnesoid X receptor induces Takeda G-protein receptor 5 cross-talk to regulate bile acid synthesis and hepatic metabolism. J Biol Chem. 2017 Jun 30;292(26):11055–69.

63. Kim I, Ahn S-H, Inagaki T, Choi M, Ito S, Guo GL, Kliewer SA, Gonzalez FJ. Differential regulation of bile acid homeostasis by the farnesoid X receptor in liver and intestine. J Lipid Res. 2007 Dec;48(12):2664–72.

64. Kleiner DE, Brunt EM, Van Natta M, Behling C, Contos MJ, Cummings OW, Ferrell LD, Liu Y-C, Torbenson MS, Unalp-Arida A, Yeh M, McCullough AJ, Sanyal AJ, Nonalcoholic Steatohepatitis Clinical Research Network. Design and validation of a histological scoring system for nonalcoholic fatty liver disease. Hepatology. 2005 Jun;41(6):1313–21.

65. Diehl AM, Day C. Cause, pathogenesis, and treatment of nonalcoholic steatohepatitis. N Engl J Med. 2017 Nov 23;377(21):2063–72.

66. Tuganbaev T, Mor U, Bashiardes S, Liwinski T, Nobs SP, Leshem A, Dori-Bachash M, Thaiss CA, Pinker EY, Ratiner K, Adlung L, Federici S, Kleimeyer C, Moresi C, Yamada T, Cohen Y, Zhang X, Massalha H, Massasa E, Kuperman Y, Elinav E. Diet Diurnally Regulates Small Intestinal Microbiome-Epithelial-Immune Homeostasis and Enteritis. Cell. 2020 Sep 17;182(6):1441-1459.e21.

67. Chen J, Vitetta L. Gut microbiota metabolites in NAFLD pathogenesis and therapeutic implications. Int J Mol Sci. 2020 Jul 23;21(15).

68. Kohsaka A, Laposky AD, Ramsey KM, Estrada C, Joshu C, Kobayashi Y, Turek FW, Bass J. High-fat diet disrupts behavioral and molecular circadian rhythms in mice. Cell Metab. 2007 Nov;6(5):414–21.

69. Hoyles L, Fernández-Real J-M, Federici M, Serino M, Abbott J, Charpentier J, Heymes C, Luque JL, Anthony E, Barton RH, Chilloux J, Myridakis A, Martinez-Gili L, Moreno-Navarrete JM, Benhamed F, Azalbert V, Blasco-Baque V, Puig J, Xifra G, Ricart W, Dumas M-E. Molecular phenomics and metagenomics of hepatic steatosis in non-diabetic obese women. Nat Med. 2018 Jul;24(7):1070–80.

70. Diastix Reagent Strips for Urinalysis | Total Diabetes Supply [Internet]. [cited 2021 Feb 22]. Available from: https://www.totaldiabetessupply.com/products/bayer-diastix-reagent-strip-for-urine-glucose-50ct?gclid=CjwKCAiAyc2BBhAaEiwA44-wWzN7Rt0mWUo3GqUDQAOMFHVt0qOSDORVMxdh0833bIwjmksXeuP0hxoCtAoQAvD_BwE

71. Promethion Cages - Sable Systems International [Internet]. [cited 2021 Feb 22]. Available from: https://www.sablesys.com/products/promethion-line/promethion-cages/

72. 16S Illumina Amplicon Protocol : earthmicrobiome [Internet]. [cited 2022 Sep 12]. Available from: http://earthmicrobiome.org/protocols-and-standards/16s/

73. Caporaso JG, Lauber CL, Walters WA, Berg-Lyons D, Huntley J, Fierer N, Owens SM, Betley J, Fraser L, Bauer M, Gormley N, Gilbert JA, Smith G, Knight R. Ultra-high-throughput microbial community analysis on the Illumina HiSeq and MiSeq platforms. ISME J. 2012 Aug;6(8):1621–4.

74. Shaffer JP, Marotz C, Belda-Ferre P, Martino C, Wandro S, Estaki M, Salido RA, Carpenter CS, Zaramela LS, Minich JJ, Bryant M, Sanders K, Fraraccio S, Ackermann G, Humphrey G, Swafford AD, Miller-Montgomery S, Knight R. A comparison of DNA/RNA extraction protocols for high-throughput sequencing of microbial communities. BioTechniques. 2021 Mar;70(3):149–59.

75. Gonzalez A, Navas-Molina JA, Kosciolek T, McDonald D, Vázquez-Baeza Y, Ackermann G, DeReus J, Janssen S, Swafford AD, Orchanian SB, Sanders JG, Shorenstein J, Holste H, Petrus S, Robbins-Pianka A, Brislawn CJ, Wang M, Rideout JR, Bolyen E, Dillon M, Knight R. Qiita: rapid, web-enabled microbiome meta-analysis. Nat Methods. 2018 Oct 1;15(10):796–8.

76. QIIME 2 user documentation — QIIME 2 2020.11.1 documentation [Internet]. [cited 2021 Feb 22]. Available from: https://docs.qiime2.org/2020.11/

77. Aron AT, Gentry EC, McPhail KL, Nothias L-F, Nothias-Esposito M, Bouslimani A, Petras D, Gauglitz JM, Sikora N, Vargas F, van der Hooft JJJ, Ernst M, Kang KB, Aceves CM, Caraballo-Rodríguez AM, Koester I, Weldon KC, Bertrand S, Roullier C, Sun K, Dorrestein PC. Reproducible molecular networking of untargeted mass spectrometry data using GNPS. Nat Protoc. 2020 Jun;15(6):1954–91.

78. Dührkop K, Fleischauer M, Ludwig M, Aksenov AA, Melnik AV, Meusel M, Dorrestein PC, Rousu J, Böcker S. SIRIUS 4: a rapid tool for turning tandem mass spectra into metabolite structure information. Nat Methods. 2019 Apr;16(4):299–302.

79. Dührkop K, Nothias L-F, Fleischauer M, Reher R, Ludwig M, Hoffmann MA, Petras D, Gerwick WH, Rousu J, Dorrestein PC, Böcker S. Systematic classification of unknown metabolites using high-resolution fragmentation mass spectra. Nat Biotechnol. 2021 Apr;39(4):462–71.

80. Govindarajan K, MacSharry J, Casey PG, Shanahan F, Joyce SA, Gahan CGM. Unconjugated Bile Acids Influence Expression of Circadian Genes: A Potential Mechanism for Microbe-Host Crosstalk. PLoS ONE. 2016 Dec 1;11(12):e0167319.

81. Zhang Y, Park C, Bennett C, Thornton M, Kim D. Rapid and accurate alignment of nucleotide conversion sequencing reads with HISAT-3N. Genome Res. 2021 Jun 8;

82. Shumate A, Wong B, Pertea G, Pertea M. Improved transcriptome assembly using a hybrid of long and short reads with StringTie. PLoS Comput Biol. 2022 Jun 1;18(6):e1009730.

83. Love MI, Huber W, Anders S. Moderated estimation of fold change and dispersion for RNA-seq data with DESeq2. Genome Biol. 2014;15(12):550.

84. Zhou Y, Zhou B, Pache L, Chang M, Khodabakhshi AH, Tanaseichuk O, Benner C, Chanda SK. Metascape provides a biologist-oriented resource for the analysis of systems-level datasets. Nat Commun. 2019 Apr 3;10(1):1523.